THERMAL AND STRUCTURAL CONSTRAINTS ON THE TECTONIC EVOLUTION OF THE IDAHO-WYOMING-UTAH THRUST BELT

A Thesis

by

SHAY M CHAPMAN

Submitted to the Office of Graduate Studies of
Texas A&M University
in partial fulfillment of the requirements for the degree of

MASTER OF SCIENCE

Chair of Committee,	Brent V. Miller
Committee Members,	Franco Marcantonio
	Robert Korty
Head of Department,	John R. Giardino

August 2013

Major Subject: Geology

ABSTRACT

The timing of motion on thrust faults in the Idaho-Wyoming-Utah (IWU) thrust belt comes from synorogenic sediments, apatite thermochronology and direct dating of fault rocks coupled with good geometrical constraints of the subsurface structure. The thermal history comes from the analyses of apatite thermochronology, thermal maturation of hydrocarbon source rocks and isotope analysis of fluid inclusions from syntectonic veins. New information from zircon fission track and zircon (U-Th)/He analysis provide constraints on the thermal evolution of the IWU thrust belt over geological time. These analyses demonstrate that the time-temperature pathway of the rocks sampled never reached the required conditions to reset the thermochronometers necessary to provide new timing constraints. Previous thermal constraints for maximum temperatures of IWU thrust belt rocks, place the lower limit at ~110°C and the upper limit at ~328°C. New zircon fission track results suggest an upper limit at ~180°C for million year time scales. ID-TIMS and LA-ICPMS of syntectonic calcite veins suggest that new techniques for dating times of active deformation are viable given that radiogenic isotope concentrations occur at sufficient levels within the vein material.

DEDICATION

I would like to dedicate this thesis to my friends and family that have supported me in my decision to continue my education. My choice to pursue higher education was encouraged by a few select friends that had confidence in my abilities when I had come to a cross-road in my life. I am thankful for the words over the years as many obstacles to my education threatened to delay and inhibit my goals.

ACKNOWLEDGEMENTS

I would like to thank my former committee chair, Dr. David Wiltschko for all of his effort that contributed to this research and encouraged me to think about the scientific problems from different perspectives. His influence, knowledge and personality were sorely missed following his passing. I would like to thank Dr. Brent Miller for his willingness to replace Dr. Wiltschko as my committee chair and taking on the difficult task of finding a way to finish this research project. His advice and edits were invaluable as well as his support in the laboratory for the vein analyses. I would also like to thank Dr. John Spang for helping me with the structural interpretation of my cross-sections. I would also like to thank my committee members, Dr. Franco Marcantonio and Dr. Robert Korty who joined my committee late in my project and on short notice, they have my sincerest gratitude.

I would like to thank Dr. John "Rick" Giardino for finding a way to keep me financially supported during the completion of this project. I would like to thank Dr. Stuart Thomson (University of Arizona) for performing the zircon and apatite fission track analysis. I would like to thank Dr. Daniel Stockli and Roman Kislitsyn (University of Texas) for conducting the zircon (U-Th)/He analysis. I would like to thank Harold Johnson for aiding me on my sample collection and his invaluable help with this project. I would like to thank all the faculty and staff at Texas A&M University that aided me along the way and contributed to my research and education. I would like to

acknowledge the M. T. Halbouty Chair in geology to Dr. David Wiltschko that partially funded this project.

TABLE OF CONTENTS

Page

1. INTRODUCTION

The thermal history and tectonic evolution of the Idaho-Wyoming-Utah (IWU) thrust belt is largely constrained by cross-cutting relationships, inferred thermal structure, and the dating of synorogenic sediments (e.g. Armstrong and Oriel, 1965; Royce et al., 1975; Jordan, 1981; Wiltschko and Dorr, 1983; Burtner and Nigrini, 1994; DeCelles, 1994). These techniques are useful for bracketing the duration a thrust fault was active but represent a loose age constraint, and favors the younger portion of the thrust belt, which preserves a more complete history. As the evolution of the fold and thrust belt progresses much of the early sedimentary record may be removed due to erosion as the previously deposited material is uplifted and exposed.

Thermochronology has been shown to be a useful technique for constraining the timing of thrust fault motion when used in conjunction with well constrained fault geometries, for example in Taiwan (Rodriguez-Roa and Wiltschko, 2006; Wiltschko et al., 2007; Lock and Willett, 2008). Multiple thermochronological techniques may be used in conjunction to provide both timing and temperature information. In the IWU, Burtner and Nigrini (1994) focused on evaluating the tectonic and thermal history in order to understand hydrocarbon maturation and the timing of migration. Their study was based on apatite fission track analysis as well as several organic maturation techniques to constrain temperature and timing.

This study was conducted with the purpose of using low temperature thermochronological techniques to add further temperature and timing constraints to the

previous work done by Burtner and Nigrini (1994). Additionally, new retro-deformable balanced cross-sections were drawn to provide a tectonic framework to better understand the significance of the thermal and tectonic history of the IWU thrust belt.

2. GEOLOGICAL OVERVIEW

2.1 Thrust Belt Geology

The Idaho-Wyoming-Utah (IWU) fold and thrust belt is a series of roughly north-south striking, west dipping thrust faults that were active during the early Cretaceous through the early Eocene and formed as part of the Sevier orogeny (Fig. 1). The regional structures form a convex to the east salient approximately 300 km long and 100 km wide, extending from southeastern Idaho, south into Utah and east into western Wyoming (Fig. 2). The thrust belt consists of six major thrust faults: the Paris-Willard, Meade, Crawford, Absaroka, Darby (Hogsback), and Prospect as well as many minor faults and folds (Fig. 2). The thrust faults generally display ramp and flat geometries and decrease in spacing from hinterland to foreland (e.g. Armstrong and Oriel, 1965; Royse et al., 1975).

The IWU fold and thrust belt is a thin skinned thrust system that is mostly made up of passive margin sediments deposited during the Neoproterozoic through the late Jurassic. Sediment thicknesses increase toward the west as the sequences were deposited off the craton. Synorogenic sediments sourced by the uplifted passive margin sediments were deposited in the down-warped foreland basins as the orogeny progressed, mostly during the Cretaceous. Many of the synorogenic units were then cut by younger thrust faults as the thrust system advanced eastward.

The faults progressively get younger from west to east and decrease in dip towards the foreland. The thickest thrust sheets are carried by the oldest thrust faults and become thinner to the east towards the younger faults. The faults are in sequence from west to east with a few minor exceptions most notably the Prospect fault (Armstrong and Oriel, 1965; Royce et al., 1975; Jordan, 1981, Lamerson, 1982). Detachments occur in weak Mesozoic and Paleozoic horizons and cut upward through younger stronger rocks. The Paris-Willard is the oldest fault in the sequence, was active the longest (Jordan, 1981; Wiltschko and Dorr, 1983) and is thought to have reinitiated several times after periods of inactivity (Wiltschko and Dorr, 1983). The Paris-Willard is thought to account for a minimum of 35 km of displacement (Yonkee et al., 1989) but has the least amount of horizontal displacement, based on the quantity of erosional products, which suggests a steeper ramp that differs in structural geometry from the long basal detachments found in the younger portion (Wiltschko and Dorr, 1983).

The geology of the IWU fold and thrust belt is described by many previous studies (e.g. Armstrong and Oriel, 1965; Royse et al., 1975; Wiltschko and Dorr, 1983; DeCelles, 1994) and is represented by extensive map coverage from state surveys, published documents (e.g. Oriel and Platt, 1980; Blackstone, 1977, 1980), and USGS surveys. However, gaps exist in the data, largely the result of missing stratigraphy, due to erosion of the uplifted units. The subsurface has been interpreted from the surface geology, seismic reflection data and petroleum exploration well data. A comprehensive compiling of available data was conducted by Dixon (1982) to provide cross-sections at about a 10 kilometer spacing nearly perpendicular to the structural trends. These cross-

sections are key constraints to the structural and stratigraphic geometries and are the base reference for the cross-sections drawn in this study.

2.2 Stratigraphy

The stratigraphy of the formations within the IWU fold and thrust belt consists of three basic sequences of deposition described by previous works (Armstrong and Oriel, 1965; Coogan and Royce, 1990, DeCelles, 2004) (Fig. 3). The first stage is a passive margin wedge that was deposited from the Proterozoic through the mid-Paleozoic unconformably upon Archean basement. The base of this sequence is dominated by a shallow marine clastic sequence deposited during Neoproterozoic through mid-Cambrian time and thickens westward upon the ancestral shelf of the North American craton. The sequence deposited from the mid-Cambrian through Devonian is dominated by carbonates with interbedded shales and sandstones.

The second phase of deposition is the tectonically influenced eastward shift that occurred from the Mississippian through the Jurassic. The tectonic events attributed to the shift of the depositional center include the Antler Orogeny (Speed and Sleep, 1983), the Ancestral Rockies (Jordan and Douglass, 1980), the Sonoma event (Paull and Carr, 1983), and the Manning Canyon detachment (Allmendinger and Jordan, 1981; Wiltschko and Dorr, 1983).

The third phase is the deposition of clastic synorogenic sediments into the foreland basins that began forming in the early Cretaceous and continued into the

Eocene as the Sevier orogeny transitioned into the Laramide orogeny and shifted eastward. The foreland basins were created by the loading and resultant down-warping of the crust caused by the progression of thrust sheets. Many of these deposits were incorporated into the hanging walls of the progressing thrust fronts. It is the age of these deposits that provide the key age constraints on the timing of thrust events (e.g. Royse et al., 1975; Wiltschko and Dorr, 1983; Heller et al., 1986; DeCelles et al., 1993; DeCelles, 1994)

2.3 Timing

Much of what is known about the times at which the IWU thrust faults were active come from the information derived from the synorogenic sediments (e.g. Armstrong and Oriel, 1965; Royse et al., 1975; Wiltschko and Dorr, 1983; Heller et al., 1986; DeCelles, 1994). Much of the work done in the thrust belt in the 1960's through the 1980's provided good constraints of the younger faults since the more recent sediments are relatively well preserved and show cross-cutting relationships that can be tied together with the tectonic events (e.g. Armstrong and Oriel, 1965; Royse et al., 1975; Wiltschko and Dorr, 1983). Correlations between paleontological information from the synorogenic sediments, sediment sourcing and the cross-cutting relationships improved the bracketing on the times at which thrust faults were actively in motion (Wiltschko and Dorr, 1983). However, paleontological constraints have inherent limitations. The age range of some fossils spans the times of active faulting and provide

a range that may not directly constrain the onset or termination of activity with sufficient accuracy. Synorogenic sediments, like conglomerates and other coarse sediments are typically poor rock types for fossil preservation. Correlating sedimentary packages with fault movements can also be difficult when, for example, it is not directly known if more than one fault was active at a given time. Attributing clasts found in synorogenic sediment to formations exposed by faults may also be difficult if more than one fault exposes the same formation and clasts may be sourced from either exposure.

Recent success with using thermochronology methods to constrain more accurately the timing of motion on thrust belts include Taiwan (Rodriguez-Roa and Wiltschko, 2006; Wiltschko et al., 2007; Lock and Willett, 2008) and the Andes (Barnes et al., 2006; Parra et al., 2009). Rodriguez-Roa and Wiltschko (2006) demonstrated how the mechanics, kinematics and fault geometries can be determined with the aid of thermochronology to build a structural model of thrust belt development. Lock and Willett (2008) presented a 2 dimensional model that predicts the pattern expected for the resetting and tracking of thermochronological indicators in thrust belts (Fig. 4). It couples a kinematic and thermal model that demonstrates the relationship between the rate of exhumation and the predicted age of the thermal event, in this case apatite fission track and (U-Th)/He. Using a 2D model of a fault bend fold, Lock and Willett (2008) demonstrate that a ‘U-shaped’ pattern will form when the geometry and displacement is known (Fig. 4). The oldest ages, labeled 1 and 3 (Fig. 4) bound the beginning and end of thrust motion and the youngest ages labeled 2 (Fig. 4) can be used to estimate the rate of motion. This ‘U-shaped’ model can be used as a general predictor that can be applied to

other thrust belts to interpret the current estimates of deformation. Because the IWU thrust belt has a well constrained structural geometry and rocks that were likely buried deeply enough to reset low-T thermochronometers this model should help to constrain the deformation history.

Thermochronology (Burtner and Nigrini, 1994) and the direct dating of fault rocks (Solum and van der Pluijm, 2007) in the IWU have introduced some newer and more precise constraints. The thermochronology by Burtner and Nigrini (1994) is sparse in the older portion of the IWU thrust belt and is limited in the direct timing constraints it provides but it does demonstrate the potential of thermochronology in the IWU thrust belt. The direct fault dating by Solum and van der Pluijm (2007) seems to indicate viable dates but is only available in the younger portion of the thrust belt which does have the most accurate timing constraints. It also indicates the very end of fault motion where thermochronology would demonstrate a time period of active motion.

2.4 Thermal History

The thermal history of the IWU thrust belt is complicated and unresolved. Many of the measured temperature constraints seem to be inconsistent with burial alone and require a component of tectonic or hydrodynamic heating (Burtner and Nigrini, 1994; DeCelles, 2004). Higher temperatures than would be expected through burial and standard geothermal gradients (~25°C/km) are found in several studies and different parts of the thrust belt (Edman and Surdam, 1984; Warner and Royce, 1987; Yonkee et

al., 1989, Burtner and Nigrini, 1994; Wiltschko et al., 2009). This suggests that assumptions about using standard geothermal gradients in dynamic systems such as those found in thrust regimes may not be entirely viable.

One of the key lines of evidence for elevated geothermal gradients is the thermal maturity of the hydrocarbon producing unit of the Phosphoria Formation. The Phosphoria is a Permian age unit that includes interbedded dark shale, phosphorite, carbonate and sandstone. Studies conducted on the Phosphoria have shown that it is consistently overmature in most places in the thrust belt (Edman and Surdam, 1984; Warner and Royce, 1987; Burtner and Nigrini, 1994), indicating temperatures in the formation above 150°C. Attributing a geothermal gradient based on estimated overburden thickness and extrapolating the estimated geothermal gradient deeper puts many of the older units below the Permian (Fig. 3) in the zircon partial annealing zone.

Burtner and Nigrini (1994) recognized higher temperatures in shallower Cretaceous hydrocarbon producing units during the thrusting along Paris-Willard system (Fig. 5). They attributed the higher temperatures to the hydrodynamic system in the basin. They inferred that meteoric rain water that fell on the newly formed mountain front would depress gradients near the thrust sheet and then the fluids would migrate to deeper parts of the basin collecting heat and then releasing that heat to shallower regions on the opposite side of the foredeep as fluids migrated towards the basin margins. Motion on the Meade and Crawford fault systems would have significantly reduced this effect by cutting off the hydrodynamic system. Therefore, the higher geothermal gradients were temporary and may not have contributed higher temperatures to

formations outside of the hydrodynamic system. Other basins in the thrust belt may also have had higher geothermal gradients on the eastern margins based on the hydrodynamic system but would have been on a smaller scale as subsequent basins were smaller in area.

Burtner and Nigrini (1994) also provide a thermal profile from the Gulf 1 Huff Lake Federal Well located on the Crawford thrust sheet (Fig. 6). This profile (Fig. 5) is based on the measured temperatures in the well and data acquired from apatite fission track (AFT) lengths and thermal maturity. The data were modeled to account for variations in formation thickness, stratigraphic ages, physical properties of lithological units, the measured downhole temperatures and basal heat flow. The basal heat flow was adjusted to fit between modeled and calculated values. In order for the modeled values to fit the maturation data and AFT dates and lengths temperatures had to be significantly increased prior to movement on the Crawford thrust by ~20 m.y. Extrapolating their average geothermal gradient of 45.6°C/km to formations deeper stratigraphically would put them well within the partial annealing zone for zircon fission tracks (ZFT). However, their premise suggest that the hydrodynamic system was likely confined to particular formations that acted as conduits for fluid flow and may not have contributed to the overall geothermal gradient.

Another indicator of high geothermal gradients in the IWU thrust belt comes from estimated formation temperatures of fluid inclusions found in syntectonic veins (Yonkee et al., 1989; Wiltschko et al., 2009). Wiltschko et al. (2009) examined syntectonic veins from the foot wall of the Absaroka thrust. They found that fluid

inclusion entrapment temperatures were between 175-328°C based on estimated overburden thickness and the fluid inclusion analysis results. Fluid inclusions should record the temperature of vein-forming fluids at that depth at the time of formation. Yonkee et al. (1989) examined homogenization temperatures of veins taken from the Willard thrust. They found a bimodal distribution of temperatures in one sample with peaks at ~180°C and ~260°C and a unimodal distribution in another with a peak at ~200°C.

3. RETRO-DEFORMABLE CROSS-SECTIONS

Many regional cross-sections have been drawn through the IWU fold and thrust belt and include: Royce et al., 1975; Dixon, 1982; Lamerson, 1982; Coogan, 1992. Extensive mapping of the exposed surface units in the IWU region provides good coverage of surface geology enabling the initial geometrical constraints for creating cross-sections. Sub-surface information has come mostly from seismic surveys and well data acquired during petroleum exploration and is incorporated into the published cross-sections.

Dixon (1982) created cross-sections that were used in this study as the initial reference. Dixon (1982) used available surface geology and subsurface geology to create a series of 47 cross-sections at roughly 10 km spacing perpendicular to structural trends. Some of Dixon's pre-published larger more detailed versions of the cross-sections were available at TAMU acquired previously through personal contact by Dr. David Wiltschko. Previously unpublished regional cross-sections drawn by Lamerson around 1980 were also acquired previously through personal contact by Dr. David Wiltschko and were available at TAMU and provide additional constraints and interpretations.

3.1 Cross-section Methods

The locations of cross-sections for this study were selected based on several key criteria. The initial goal was to provide a representative regional coverage of the thrust

belt so that all the major thrust sheets and faults would be included in the cross-sections. The selection criteria included an effort to maximize constraints provided by the previous published cross-sections and those available at TAMU. It was also important to avoid areas of structural complexity within the thrust belt that may limit the usefulness of new timing constraints. Secondly, it was important to try to incorporate as much of the available thermochronology data from the apatite fission track work of Burtner and Nigrini (1994). Additionally, knowledge of the landscape was important as access to exposed outcrop for sampling by road would be critical. Several early selections were discarded as being inaccessible for sample collection. Selections in the southern portion of the IWU thrust belt would inhibit sample collection from each major thrust sheet due to sediment cover.

Cross-sections were drawn using the Midland Valley *Move* software and imported maps and figures acquired from various sources. An elevation surface map acquired from the USGS online map database was used to project the topographic surface (National Elevation Dataset, 2009). Faults surface locations were projected onto topography using the intersections of faults with the topographic surface. Faults were taken from a digital geo-referenced geological map also acquired from the USGS online map database (USGS, 2008). After the fault locations were projected onto the topographic surface Dixon's (1982) published cross-sections were imported and modified to fit as closely as possible to those projections to create an initial frame of reference for cross-section construction. The imported sections were stretched to match the scale in *Move* and horizontally stretched to match the geo-referenced topography and

fault locations, thus creating a geo-referenced cross-section guide in order to best honor the published geometrical constraints. Dixon's (1982) sections were thought to incorporate the most subsurface constraints available; however some of the complex structural interpretations in the subsurface geometries had to be simplified in order for balancing and restoration to be viable.

Move's "fault parallel flow" algorithm was used for most of the restoration process as this allowed for units to return to a parallel orientation as they crossed from ramp to flat. The "trishear" algorithm was used to forward model some of the fault propagated folds and subsequently restore them. The series of faults and folds as they were drawn required repeated modeling attempts to move the faults from drawn to restored segment to allow the cross-sections to properly align and balance. Sedimentary units are known to thicken to the west but were kept at a mostly constant thickness during cross-section construction as it is difficult to vary unit thickness in the software and maintain structural geometry during the restoration process.

3.2 Cross-section Discussion

Simplifications for the purpose of generating retrodeformable cross-sections (Fig.7, 8, 9) include; assigning a generally uniform unit thickness (Fig. 3), elimination of minor folds and faults, and reduction of some complexities when the geometries could not be resolved. The restoration also involved slight adjustments to the shapes of ramps and the position of flats inferred by Dixon (1982). The original goal was to create retro-

deformable sections in which any surface point could be restored to the depth indicated by the thermochronology closure temperature at the time indicated by the thermochronometer and thus the thermal and structural evolution of the thrust. However, contrary to expectations, temperatures were not high enough to reset zircon fission track ages so sections were restored to horizontal along the basal detachments (Fig. 7, 8, 9) without timing constraints.

4. THERMOCHRONOLOGY AND RECONNAISSANCE GEOCHRONOLOGY

This study used the techniques of apatite fission track (AFT) dating, zircon fission track dating (ZFT), zircon (U-Th)/He dating (ZHe), and calcite vein radiometric dating (CVR) with the intent of constraining the timing of thrust related cooling, exhumation and syntectonic vein formation. The AFT, ZFT and Zhe methods record the time at which the rock cooled through a mineral closure temperature (Fig. 10). If temperatures remain above the closure temperature for a sufficient amount of time to reset the previous closure then the crystal is reset and records the latest heating event. The processes that reset the thermochronometers do not occur at constant rates (Fig. 10) so ages must be combined with temperature and/or kinematic models to recreate a rock's thermal history. CVR U-Pb dating is based on the assumption that vein fill materials crystallize from fluids moving within fractures during syntectonic deformation caused by motion on faults.

4.1 Thermochronology Methods

Apatite fission track (AFT) dating has an approximate closure temperature of 110°C ±10 with the partial-annealing zone where tracks may partially heal down to as low as 60°C assuming cooling rates along normal crustal geothermal gradients (Donelick et al., 2005). Fission tracks anneal at variable temperature conditions based on the ability to diffuse radiation-induced crystal lattice defects through the crystal which will occur

faster at higher temperatures. Apatite composition, mainly Cl, F, and OH content, also affects the annealing process. Chloro-apatite has been shown to be more resistant to annealing and has better fission track retention than that of Fluoro-apatite (Burtner et al., 1994; Gallagher et al., 1998; Reiners, 2006) but an analysis can be calibrated using equations derived from apatite annealing models (Ketchum, 2005; Ketchum et al., 2006) that includes the more resistant types of apatite annealing. AFT was conducted on a single sample at the University of Arizona fission track laboratory. The sample was prepared using standard mineral separation techniques after Donelick et al., (2005) and follows the method of Thomson, (2002).

Zircon fission track (ZFT) dating has an approximate closure temperature of 240°C ±20 (Brandon et al., 1998). Similar to apatite the amount of annealing depends on the time-temperature history of the crystal. The temperatures that zircon anneals is variable based on fission damage dosage which is a function of its age and U concentration. Zircons with significant amounts of radiation damage anneal more quickly and have a lower annealing temperature than those that do not (Brandon et al., 1998) (Fig. 10). Generally the older the zircon grain the more likely it is to have higher radiation damage given a high enough uranium concentration. In previous studies higher annealing temperatures were likely due to the low radiation decay damage in young zircons (Brandon et al., 1998). ZFT was conducted on fifteen samples at the University of Arizona fission track laboratory. The sample was prepared using standard mineral separation techniques after Donelick et al., (2005).

Zircon (U-Th)/He (Zhe) dating is a useful thermochronometer in the temperature range of 140°-210°C (Reiners et al., 2002; Stockli, 2005; Biswas et al., 2007). This method is based on trapping the alpha-decay produced ^{4}He nucleus within the crystal lattice that results from decay of the isotopes uranium, thorium, and samarium. The rate at which radiogenic helium diffuses out of the mineral is a function of temperature and cooling rate (Reiners and Brandon, 2006).

Six zircons each from six samples collected in proximity to cross-section C-C' (Fig. 6) were analyzed using the (U-Th)/He thermochronometric technique at the University of Texas at Austin (U-Th)/He Geo- and Thermochronometry laboratory. Zircons were selected based on several criteria: 1) the grain is as close euhedral as is available in the sample; 2) the grain is free of inclusions that contain U and Th; 3) grain has a width of no less than 70 μm. The selected single zircon grains were placed in platinum tubes and laser heated to 1300°C then reheated to ensure complete degassing. Extracted He was spiked with ^{3}He tracer and analyzed in a computer automated UHV He extraction line and a Blazers Prisma QMS-200 quadrupole mass spectrometer that measures ^{3}He/^{4}He ratios. Zircons were dissolved using standard U-Pb double pressure-vessel digestion procedures (HF- HNO3 and HCl). Solutions were spiked with ^{230Th}, ^{235}U, ^{149}Sm and REE tracer and analyzed for U, Th, and Sm using the Thermo Element2 HR-ICP-MS, fitted with a CETAC micro-concentric nebulizer and ESI autosampler (Wolfe and Stockli, 2010).

Data reduction was done by in-house software at the University of Texas. Measurement errors are included in the analytical methods with He being 0.3-0.5% and

U, Th, and Sm at <1-2%. Uncertainties associated with a-ejection corrections related to the distribution assumptions propagate errors of 3-4%, 2-s and underestimate reproducibility. So a value of ~8% for zircon is assigned based on population standard deviation based on replicate analysis of an age standard sample.

4.2 Reconnaissance Geochronology Methods

Vein U-Pb dating was conducted on two samples previously collected by Dr. David Wiltschko from a syntectonic vein set near Laketown Canyon, Utah, from the Mississippian Monroe Canyon limestone (Fig. 6) as a test of the viability of U-Pb calcite vein dating. These samples were analyzed by isotope-dilution, thermal ionization mass spectrometry (ID-TIMS) at Texas A&M University. Reconnaissance trace element analysis were done by laser-ablation, inductively coupled plasma mass spectrometry (LA-ICPMS) on a single sample collected along cross-section C-C' (Fig. 6), from the Permian-Pennsylvanian Wells limestone.

Two samples for ID-TIMS dating were prepared by initially cutting vein material from the whole rock sample. Material was physically crushed in an enclosed and clean container and finely ground using a mortar and pestle and sieved for a grain size of 0.5-1 mm. Grains were individually selected under microscope to be free of contaminates. Samples were weighed then washed with H20 and dissolved in 6M HCl and the solution was spiked with ^{205}Pb, ^{233}U, and ^{235}U. Both Pb and U were purified by anion exchange chemistry using 0.5M HBr and 6M HCl respectively and then evaporated by a small

drop of H3PO4 solution prior to mass spectrometry analysis. Lead isotopes were loaded in silica gel and analyzed in multiple Faraday mode. Fractionation correction of 0.12%/AMU was applied to all isotope ratios based on long-term repeat analysis of NBS981. Uranium isotopes were also loaded in silica gel and analyzed in multiple Faraday mode as the dioxide; fractionation was corrected internally based on the $^{235}U/^{233}U$ spike ratio. Isotopic data are presented in Table 4.

Another calcite vein sample collected along section C-C' (Fig. 6) was prepared for LA-ICPMS by trimming the host plus vein sample to fit in a 1" epoxy mount, lapping flat using sandpaper, and polishing to 0.25 micron diamond grit. Laser ablation analyses were conducted in a transect from host, across the vein and back into the host at a spacing of approximately 0.5 mm. Analyses were conducted at the R. Ken Williams Radiogenic Isotope Geosciences laboratory at Texas A&M University using a Photon Machines Analyte 193 excimer laser focused to a 30 micron spot with a repetition rate of 10 Hz, a fluence of 0.45 J/cm2 and He carrier gas at 0.8 LPM (liters per minute). Ablated material was analyzed on a Thermo Electron Element HR inductively-coupled-plasma mass spectrometer operating with sample gas Ar at 1.1 LPM with sample time at 90 sec. Scan type was a magnetic jump with electric scan of 3 runs and 1 pass. Search window was 150%, integration window at 20% with triple detection mode and average integration. NIST 612 glass standard was used for calibration.

4.3 Thermochronology Results

This study included AFT dating as a secondary analysis to the ZFT dating to potentially fill in areas along the chosen transects that were not covered by the Burtner and Nigrini (1994) study. There was only a single sample (Table 1) that contained enough workable apatite grains to warrant an analysis. The sample contained four grains that were feasible for fission track counting where traditionally 20 grains is used for a statistically relevant population. The four grains that were analyzed come from the Meade thrust sheet near transect 2 (Fig. 6). The average age is ~121 ± 18 Ma for the apatite grains.

Twenty two ZFT samples were processed that included at least one sample from each of the thrust sheets along the three transects selected for this study (Fig. 6). Of the twenty two samples, fifteen (Table 2) had an adequate amount of zircons of a high enough quality to warrant fission track counting. The range of ages and the associated error is highly variable and most populations represent mixed ages. All but three ages from sample WYZ 15 predate the tectonic events of the IWU fold and thrust belt.

Five samples (Table 3) were selected for Zhe dating from each thrust sheet near transect 3 (Fig. 6). Six zircons from each sample were used for the analysis to create a statistically relevant population. The ages and associated errors vary significantly within each sample. Some of the ages of individual grains fall within the timeframe of the IWU thrust belt but no consistent ages occur in a single sample. A plot of the data of effective

uranium concentration vs. age (Fig. 11) shows that the zircons with a higher U concentration tend to have a younger age.

4.4 Reconnaissance Geochronology Results

The LA-ICPMS data show a marked decline in U, Pb, and Th in proximity the vein wall and very low U and Pb concentrations within the vein itself (Fig. 12). The trend of decreasing elemental abundance for these fluid-mobile elements is interpreted to indicate leaching of the wall rock during vein emplacement; another criterion that makes U-Pb dating of veins seem more viable. The low U and Pb concentrations are not necessarily an impediment to accurate U-Pb dating. They do, however, suggest that large sample mass will be required and that ages will be limited by the line-fit statistics and spread of U/Pb ratios.

Precise CVR U-Pb ages were hampered by low U concentrations and very low ratios of radiogenic/common Pb. Calcite vein sample Olc4 has a $^{206}Pb/^{204}Pb$ ratio of 22.25 ±0.22and sample Olc12 has a $^{206}Pb/^{204}Pb$ ratio of 21.47 ±0.15 and U concentrations of 0.1108 ppm in Olc4 and 0.0007 ppm in Olc12 (Table 4). Although only two samples from the same syntectonic vein network were used for this reconnaissance analysis, the data do display a spread in U/Pb ratios and resolvable different Pb isotope compositions, the traits necessary for isochron dating. A line connecting these two data points on a 206Pb/204Pb vs. 238U/204Pb isochron diagram (Fig. 13) yields a slope consistent with initial U-Pb isotopic equilibration at 78.3 ± 5.7

Ma. Although this age is geologically sensible and within the range of ages anticipated for vein formation, it should be used only with a great deal of caution as two-point isochrons may not be reliable. The data do, however, point to the feasibility of this method as a potentially informative line of future research. Full application of this method would have required an extensive data set which fell beyond the scope of the current project.

4.5 Thermochronology Discussion

Burtner and Nigrini (1994) reported temperatures greater than 110°C in all but one of their published AFT dating samples (Fig. 6). Their samples had the inherited fission tracks completely annealed in all but one that was partially annealed. Their thermal maturation data suggested that temperatures were greater than ~150°C since most of their results showed that hydrocarbons within the Phosphoria formation were overmature for the oil window which has a maximum of ~ 150°C. With the combination of this information along with the estimated burial depths and the increase in geothermal gradients that occurs during orogenic events it was thought that temperatures should have been high enough to reset the thermochronometers used in this study.

The AFT ages of Burtner and Nigrini (1994) estimate the motion of the Meade thrust to be around 100-140 Ma and this age corresponds to the estimated sedimentological-based time of motion on the Meade ~119-90 Ma (DeCelles et al., 1993). The single apatite sample analyzed in this study (Table 1) had a mean age of 121

± 18 Ma, within the range that Burtner and Nigrini found. However, the small number of grains for this sample (four) limits the precision of the results.

All but three of the ZFT ages (Table 2) (Fig. 14) in this study predate the IWU fold and thrust belt and are highly variable in each sample. Most of the ZFT ages predate the formation of the rock unit that they are in indicating that burial temperatures never reached the time-temperature threshold to fully reset the fission tracks. However the pseudo-exponential decline when all ages are taken together (Fig. 14) may indicate a more fundamental process of partial resetting of zircon fission tracks over the IWU thrust belt as a whole. The age associated with the three anomalous ages is consistent with the 60-70 Ma cooling event found by the Burtner and Nigrini (1994) apatite analysis.

The fact that only three zircon fission track ages are reset within the time frame of IWU thrust belt activity was a completely unexpected result as all indications (described above) indicated that many of these rocks should have reached temperatures above that of zircon fission track annealing. One possibility is that these three grains were orientated along a fracture that saw abnormally hot fluids resetting just the grains that were in direct contact with the fluids.

Also unanticipated is the preservation of older Zhe dates and the broad scatter of ages with varying amounts of error; again prior work seemed to indicate that temperatures during IWU thrusting should have been hot enough to fully reset this system. The zircons with the highest concentrations of U show the youngest ages and the smaller errors. Some of the ages do fit within the timing of motion on the thrust belt but

not any single sample. One explanation for this pattern is that the zircons did reach Zhe resetting temperatures, but not for a long enough period of time to allow complete resetting. Another possible explanation is that the zircons that are partial annealed are the ones with the most inherited crystal lattice damage due to U, Th, and Sm alpha and fission decays. Having the highest U concentration in a given crystal would suggest that the fission and alpha decay damage would likely be higher. It has been shown that crystals with greater decay damage tend to anneal more readily (Brandon et al., 1998), so it seems plausible that the grains that are partial reset are the ones that carried the most inherited decay damage.

5. DISCUSSION

The thermal history of the IWU includes a dynamic and complicated set of structural and thermal events. It is clear that none of the locations sampled in this study had an adequate time-temperature pathway to fully reset the ZFT and Zhe systems. Temperatures may have exceeded the threshold for annealing and/or resetting, but were likely over too short of a time interval to fully reset the thermochronometer. Temperature recording techniques used elsewhere in the thrust belt suggest above average geothermal gradients but do not provide the time component that might explain the discrepancy that the temperature data suggests would be adequate to reset the zircons.

The apatite fission track data from Burtner and Nigrini, (2004) show that temperatures exceeded 110°C in all but one sample, similar to zircon fission tracks annealing can occur quickly if temperatures significantly exceed the partial annealing zone. This value is a maximum and does not record any event prior to cooling so it is not known for how long or how much more temperatures exceeded the annealing threshold. Based on the results of Burner and Nigrini, (1994) cooling from these temperatures was in response to uplift of thrust sheets due to tectonic motion, essentially ending the heating mechanism for the majority of units in the stratigraphic column. Burtner and Nigrini (1994) suggest later heating attributed to hydrodynamic flow but was likely confined to the shallower units deposited just before or during the progression of thrust sheets.

The overmaturity of the Phosphoria formation indicates that temperatures were at or above 150°C on at least one occasion throughout most of the IWU thrust belt. However, the thermal maturity of organic units does not require significant amounts of time to reach overmaturity, especially if the temperature threshold is exceeded. Thermal maturity records a maximum temperature the formation reached and contains no direct timing component.

Fluid inclusion temperatures recorded by Yonkee et al. (1989) in the Willard thrust sheet were as high as 260°C and by Wiltschko et al. (2009) for the Crawford thrust sheet were as high as 328°C. Syntectonic veins can form rapidly following fracture formation and emplacement of fluids moving in to the open space. Temperatures of the fluids may have been as high as reported but it is not known from where the heat was generated or the duration of residual heat. Based on apatite fission track results (Burtner and Nigrini, 1994), significant regional heating did not occur following the initiation of the Paris-Willard thrust system. Temperatures associated with fluid inclusions likely represent local conditions during vein formation.

The results from vein material analyzed by ID-TIMS demonstrate that the radiogenic dating of vein calcite may yield promising results given that high enough concentrations of radiogenic isotopes exist in the vein. LA- ICPMS analysis of vein material seems to be a convenient method for determining whether radiogenic isotope concentrations are sufficient to warrant further analysis. Individual analyses of vein material may guide sample collection from within the vein itself to increase the chance

of successful results by mapping the location of the greatest concentrations of radiogenic isotopes.

6. CONCLUSIONS

1. Zircon fission track and zircon (U-Th)/He data suggest that temperatures never reached an adequate time-temperature path to fully reset the thermochronometer.

2. The maximum temperature the majority of the rocks in the IWU thrust belt were exposed to likely occurred prior to the initiation of the Paris-Willard thrust system and temperatures were never significantly increased by burial under thrust sheets. Erosion is inferred to have maintained a close balance with uplift.

3. Maximum temperatures over geological time for the IWU thrust belt are inferred to have been between ~110°C for fully annealed apatite fission tracks and ~180 for average annealing of zircon (U-Th)/He. Any temperatures exceeding these values were for a limited duration.

4. ID-TIMS analysis of two calcite veins with low uranium content from the Crawford thrust sheet yielded dates that correspond to a time, within error, of when the Crawford sheet is thought to have been actively in motion.

5. ICPMS analysis of a calcite vein suggests that a careful mapping of radiogenic isotope concentrations in veins may be able to guide the selection of vein material that would

yield the highest concentrations for successful dating or demonstrate that values are too low to warrant further investigation of a particular sample.

REFERENCES

Allmendinger, R. W., and Jordan, T. E., 1981, Mesozoic evolution, hinterland of the Sevier orogenic belt: Geology, v. 9, no. 7, p. 308-313.

Armstrong, F. C., and Oriel, S. S., 1965, Tectonic development of the Idaho-Wyoming thrust belt: Aapg Bulletin-American Association of Petroleum Geologists, v. 49, p. 1847-1866.

Barnes, J. B., Ehlers, T. A., McQuarrie, N., O'Sullivan, P. B., and Pelletier, J. D., 2006, Eocene to recent variations in erosion across the central Andean fold-thrust belt, northern Bolivia: Implications for plateau evolution: Earth and Planetary Science Letters, v. 248, no. 1–2, p. 118-133.

Blackstone, D. L., 1977, The overthrust belt salient of the Cordilleran fold belt, western Wyoming-southeastern Idaho-northeastern Utah: *in*, Heisy, E. L., and others, eds., Rocky Mountain thrust belt; geology and resources: Wyoming Geological Association 29th Annual Field Conference Guidebook, p. 367-384.

Blackstone, D. L., and Geological Survey of Wyoming., 1980, Tectonic map of the overthrust belt, western Wyoming, southeastern Idaho and northeastern Utah: showing current oil and gas drilling and development: Geological Survey of Wyoming, scale 1:316,800.

Brandon, M. T., Roden-Tice, M. K., and Garver, J. I., 1998, Late Cenozoic exhumation of the Cascadia accretionary wedge in the Olympic Mountains, northwest

Washington State: Geological Society of America Bulletin, v. 110, no. 8, p. 985-1009.

Burtner, R. L., Nigrini, A., and Donelick, R. A., 1994, Thermochronology of lower Cretaceous source rocks in the Idaho-Wyoming Thrust belt: Aapg Bulletin-American Association of Petroleum Geologists, v. 78, no. 10, p. 1613-1636.

Burtner, R. L., and Nigrini, A., 1994, Thermochronology of the Idaho-Wyoming Thrust Belt during the Sevier Orogeny – a new, calibrated, multiprocess thermal-model: Aapg Bulletin-American Association of Petroleum Geologists, v. 78, no. 10, p. 1586-1612.

Parra, M., Mora, A., Sobel, E. R., Strecker, M. R., and González, R., 2009, Episodic orogenic front migration in the northern Andes: Constraints from low-temperature thermochronology in the Eastern Cordillera, Colombia: Tectonics, v. 28, no. 4, p. TC4004.

Coogan, J. C., and Royse, F., 1990, Overview of recent developments in thrust belt interpretation: Geologic field tours of western Wyoming and parts of adjacent Idaho, Montana, and Utah, p. 89-124.

Coogan, J. C., 1992, Structural evolution of piggyback basins in the Wyoming-Idaho-Utah thrust: Geological Society of America Memoirs, v. 179, p. 55-81.

DeCelles, P., Pile, H., and Coogan, J., 1993, Kinematic history of the Meade thrust based on provenance of the Bechler conglomerate at Red Mountain, Idaho, Sevier thrust belt: Tectonics, v. 12, no. 6, p. 1436-1450.

DeCelles, P. G., 1994, Late Cretaceous-Paleocene synorogenic sedimentation and kinematic history of the Sevier thrust belt, northeast Utah and southwest Wyoming: Geological Society of America Bulletin, v. 106, no. 1, p. 32-56.

DeCelles, P. G., 2004, Late Jurassic to Eocene evolution of the Cordilleran thrust belt and foreland basin system, western USA: American Journal of Science, v. 304, no. 2, p. 105-168.

Dixon, J. S., 1982, Regional structural synthesis, Wyoming salient of western overthrust belt: Aapg Bulletin-American Association of Petroleum Geologists, v. 66, no. 10, p. 1560-1580.

Donelick, R. A., O'Sullivan, P. B., and Ketcham, R. A., 2005, Apatite fission-track analysis: Low-temperature thermochronology: Techniques, interpretations, and applications, v. 58, p. 49-94.

Edman, J. D., and Surdam, R. C., 1984, Influence of overthrusting on maturation of hydrocarbons in Phosphoria formation, Wyoming-Idaho-Utah overthrust belt: AAPG Bulletin, v. 68, no. 11, p. 1803-1817.

Gallagher, K., Brown, R., and Johnson, C., 1998, Fission track analysis and its applications to geological problems: Annual Review of Earth and Planetary Sciences, v. 26, p. 519-572.

Heller, P. L., Bowdler, S. S., Chambers, H. P., Coogan, J. C., Hagen, E. S., Shuster, M. W., Winslow, N. S., and Lawton, T. F., 1986, Time of initial thrusting in the Sevier orogenic belt, Idaho, Wyoming and Utah: Geology, v. 14, no. 5, p. 388-391.

Hunter, R. B., 1988, Timing and structural interaction between the thrust belt and foreland, Hoback basin, Wyoming, Geological Society of America Memoirs, v. 171, p. 367-393.

Johnson, H. E., and Wiltschko, D. V., 2012, 3D Structural analysis of the Benton uplift, Ouachita orogen, Arkansas, Texas A&M University.

Jordan, T. E., and Douglass, R. C., 1980, Paleogeography and structural development of Late Pennsylvanian Early Permian Oquirrh basin, northwest Utah: Aapg Bulletin-American Association of Petroleum Geologists, v. 64, no. 5, p. 730-730.

Jordan, T. E., 1981, Thrust loads and foreland basin evolution, Cretaceous, western United-States: Aapg Bulletin-American Association of Petroleum Geologists, v. 65, no. 12, p. 2506-2520.

Ketcham, R. A., Donelick, R. A., and Carlson, W. D., 1999, Variability of apatite fission-track annealing kinetics: III. Extrapolation to geological time scales: American Mineralogist, v. 84, p. 1235-1255.

Ketcham, R. A., 2005, Forward and inverse modeling of low-temperature thermochronometry data: Low-temperature thermochronology: Techniques, interpretations, and applications, v. 58, p. 275-314.

Ketcham, R. A., Carter, A., Donelick, R. A., Barbarand, J., and Hurford, A. J., 2006, Improved measurement and modeling of fission tracks in apatite: Geochimica Et Cosmochimica Acta, v. 70, no. 18, p. A316-A316.

Lamerson, P. R., 1982, The Fossil basin area and its relationship to the Absaroka thrust fault system, *in* R. B. Powers, ed., Geological studies of the Cordilleran thrust belt, Rocky Mountain Association of Geologists, p. 279-340.

Lock, J., and Willett, S., 2008, Low-temperature thermochronometric ages in fold-and-thrust belts: Tectonophysics, v. 456, no. 3-4, p. 147-162.

Oriel, S. S., Platt, L. B., and Geological Survey (U.S.), 1980, Geologic map of the Preston 1˚ x 2˚ quadrangle, southeastern Idaho and western Wyoming: The Survey, scale 1:250,000.

Paull, R. K., and Carr, T. R., 1983, Early Triassic stratigraphy and paleogeography of the Cordilleran miogeosyncline, *in* Proceedings Mesozoic paleogeography of the west-central United States: Rocky Mountain Paleogeography Symposium 21983, Volume 2, Rocky Mountain Section, Society of Economic Paleontologists and Mineralogists, p. 39.

Reiners, P. W., 2005, Zircon (U-Th)/He thermochronometry: Low-temperature thermochronology: Techniques, interpretations, and applications, v. 58, p. 151-179.

Reiners, P. W., Ehlers, T. A., and Zeitler, P. K., 2005, Past, present, and future of thermochronology: Low-temperature thermochronology: Techniques, interpretations, and applications, v. 58, p. 1-18.

Reiners, P. W., and Brandon, M. T., 2006, Using thermochronology to understand orogenic erosion: Annual Review of Earth and Planetary Sciences, v. 34, p. 419-466.

Royce, F., Warner, M. A. and Reese, D. L., 1975, Thrust belt structural geometry and related stratigraphic problems Wyoming-Idaho-northern Utah, *in* Bolyard, D. W., ed., Deep drilling frontiers of the central Rocky Mountains: Denver, Rocky Mountain Association of Geologists. P. 41-54.

Rodriguez-Roa, F. A., and Wiltschko, D. V. 2006, A new interpretation of the thrust belt architecture of the central and southern Western Foothills, Taiwan: Geological Society of America, Abstr. W. Progr., v. 38, p. 132.

Speed, R. C., and Sleep, N. H., 1982, Antler orogeny and foreland basin – a model: Geological Society of America Bulletin, v. 93, no. 9, p. 815-828.

Solum, J. G., and van der Pluijm, B. A., 2007, Reconstructing the Snake River–Hoback River Canyon section of the Wyoming thrust belt through direct dating of clay-rich fault rocks: Geological Society of America Special Papers, v. 433, p. 183-196.

Tagami, T., Galbraith, R., Yamada, R., and Laslett, G., 1998, Revised annealing kinetics of fission tracks in zircon and geological implications, *in* Van den Haute, P., and De Corte, F., eds., Advances in fission-track geochronology: Amsterdam, Kluwer Academic Press, p. 99-112.

Thomson, S. N., 2002, Late Cenozoic geomorphic and tectonic evolution of the Patagonian Andes between latitudes 42 degrees S and 46 degrees S: An appraisal based on fission-track results from the transpressional intra-arc Liquine-Ofqui fault zone: Geological Society of America Bulletin, v. 114, no. 9, p. 1159-1173.

USGS National Elevation Dataset, open source ESRI shapefiles: http://nationalmap.gov/elevation (January, 2009).

Warner, M. A., and Royse, F., 1987, Thrust faulting and hydrocarbon generation – Discussion: Aapg Bulletin-American Association of Petroleum Geologists, v. 71, no. 7, p. 882-889.

Wiltschko, D. V., and Dorr, J. A., 1983, Timing of deformation in overthrust belt and foreland of Idaho, Wyoming, and Utah: Aapg Bulletin-American Association of Petroleum Geologists, v. 67, no. 8, p. 1304-1322.

Wiltschko, D. V., Rodriguez-Roa F. A., and Panian J., 2007, Kinematic and modeling constraints on the transition from accretion to collision in southern Taiwan: Paper #48-4, Annual Mtg., Denver, CO.

Wiltschko, D. V., Lambert, G. R., and Lamb, W., 2009, Conditions during syntectonic vein formation in the footwall of the Absaroka thrust fault, Idaho-Wyoming-Utah fold and thrust belt: Journal of Structural Geology, v. 31, no. 9, p. 1039-1057.

Wolfe, M. R., and Stockli, D. F., 2010, Zircon (U-Th)/He thermochronometry in the KTB drill hole, Germany, and its implications for bulk He diffusion kinetics in zircon: Earth and Planetary Science Letters, v. 295, no. 1-2, p. 69-82.

Yonkee, W., Parry, W., Bruhn, R., and Cashman, P., 1989, Thermal models of thrust faulting: Constraints from fluid-inclusion observations, Willard thrust sheet, Idaho-Utah-Wyoming thrust belt: Geological Society of America Bulletin, v. 101, no. 2, p. 304-313.

Yonkee, A., and Weil, A. B., 2010, Reconstructing the kinematic evolution of curved mountain belts: Internal strain patterns in the Wyoming salient, Sevier thrust belt, USA: Geological Society of America Bulletin, v. 122, no. 1-2, p. 24-49.

APPENDIX A

FIGURES/TABLES

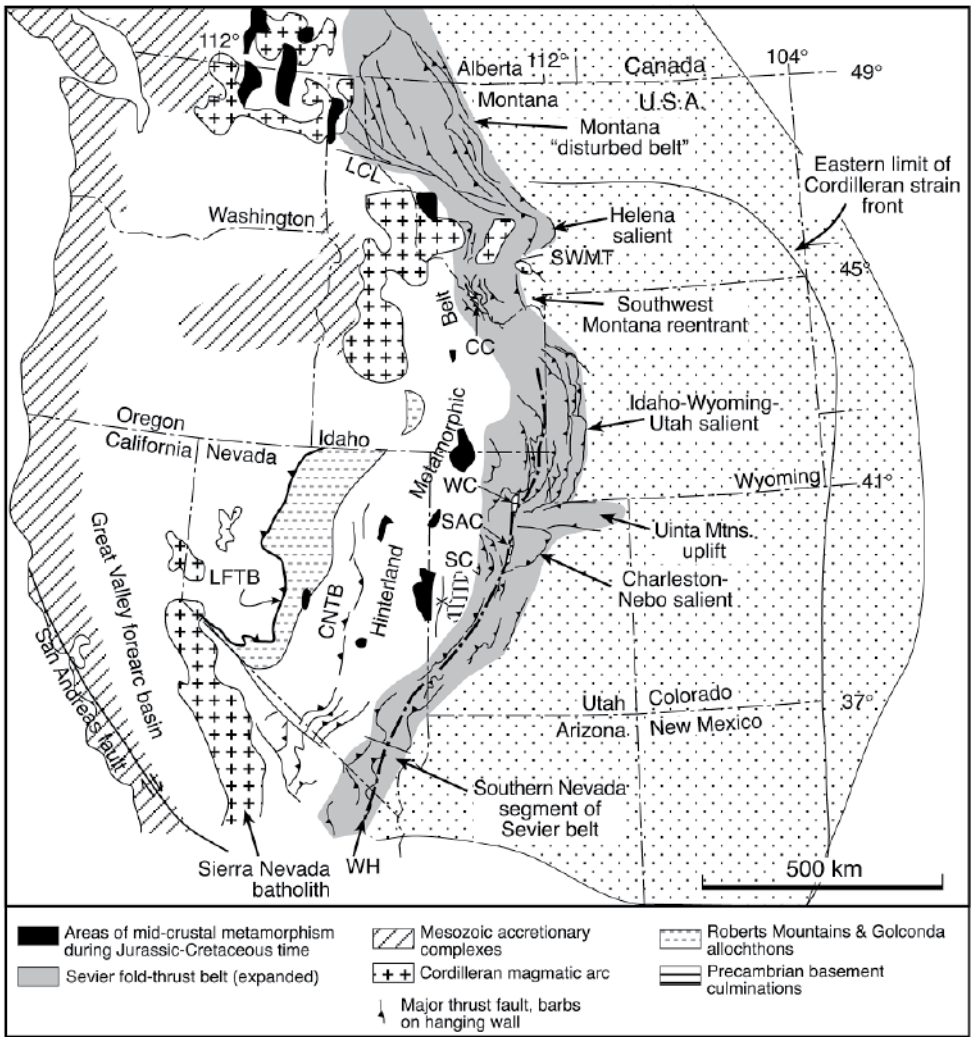

Figure 1: Tectonic overview map showing the major features associated with the Cordilleran orogenic belt (modified from DeCelles, 2004). Shaded region indicates the Sevier fold and thrust belt with the Idaho-Wyoming-Utah salient in the center. Stippled region indicates the extent of the foreland basin.

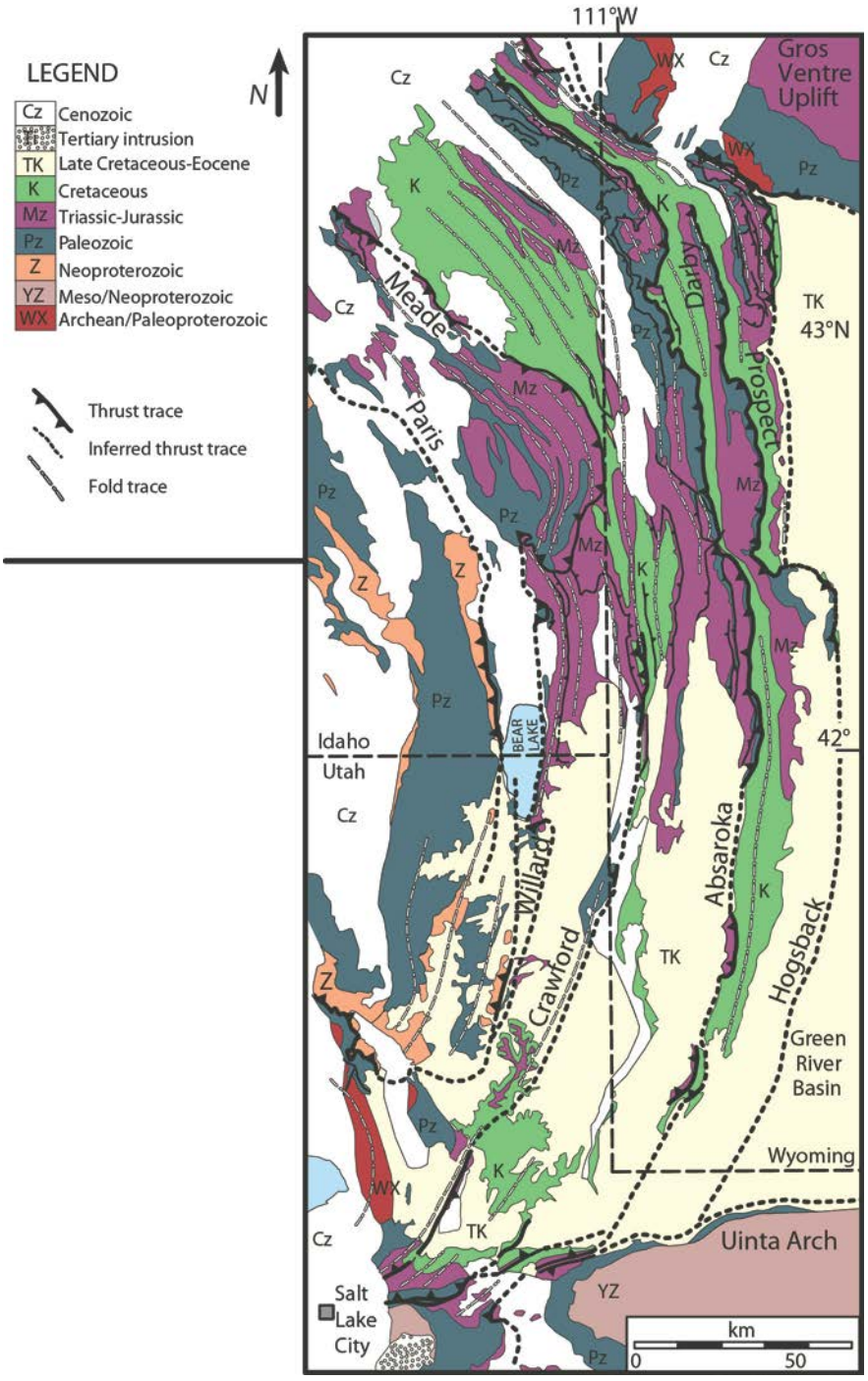

Figure 2: Generalized geological map showing the major features of the Idaho-Wyoming-Utah thrust belt (modified from Yonkee and Weil, 2010). Major thrust faults and associated folds show the regional structural trends.

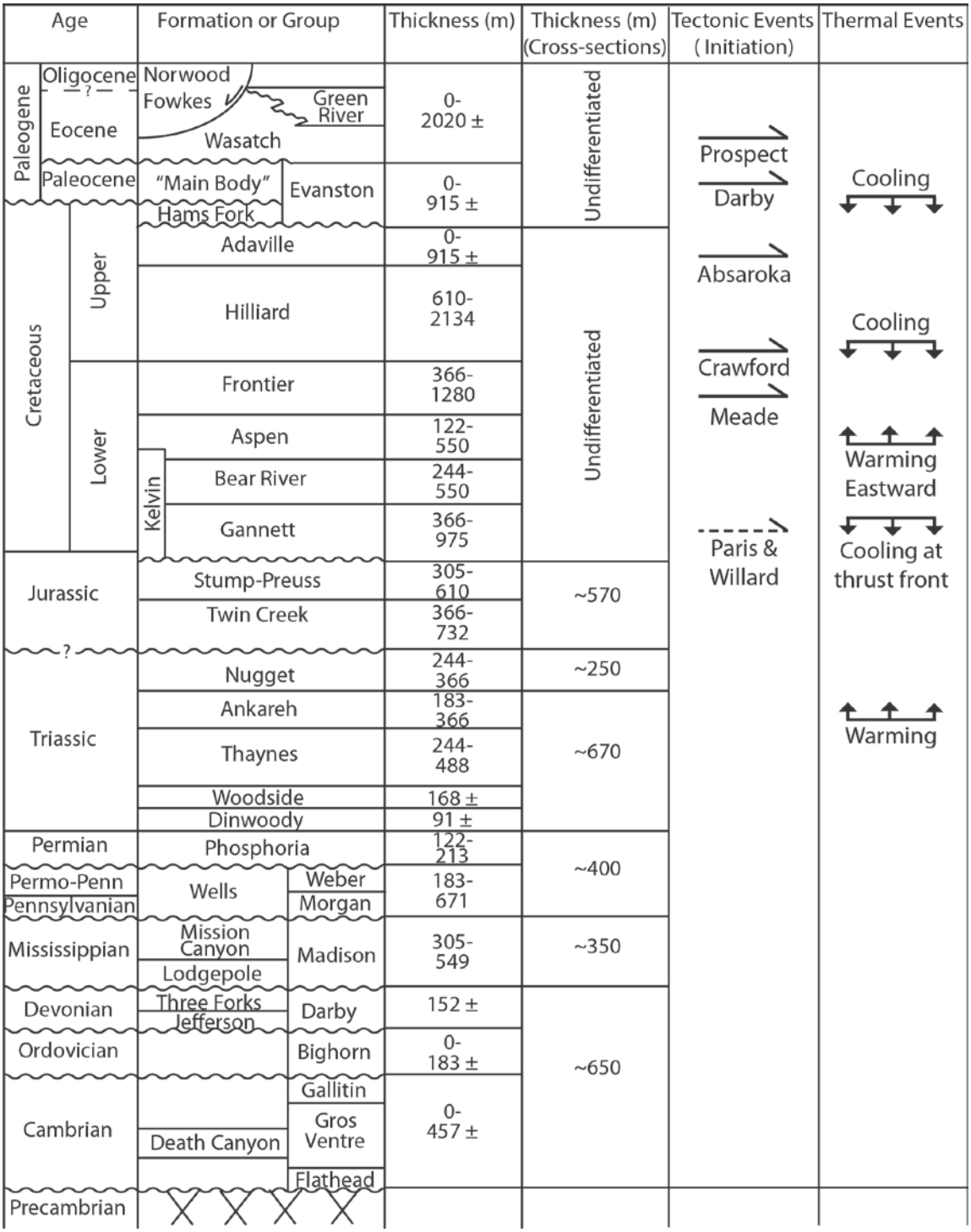

Figure 3: Simplified stratigraphic column of the general area associated with Idaho-Wyoming-Utah thrust belt (modified from Lamerson, 1982). The timing of tectonic

events inferred from (Wiltschko and Dorr, 1983; DeCelles, 1994). Thermal events inferred form (Burtner and Nigrini, 1994).

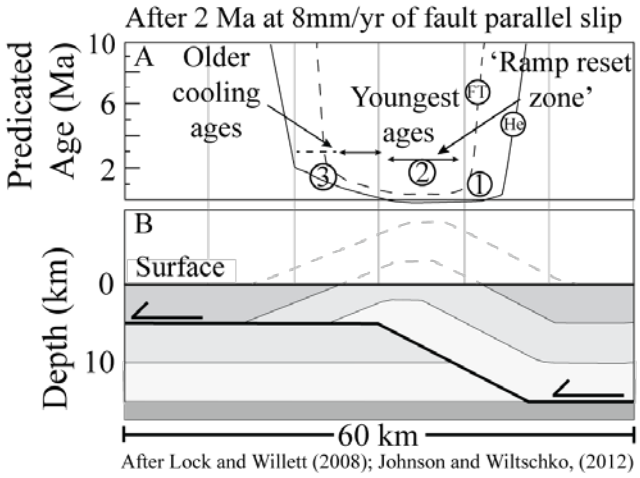

Figure 4: Model from, Lock and Willett, (2008) (modified from Johnson and Wiltschko, 2011), showing the expected ages from apatite fission track and (U-Th)/He thermochronological techniques completely eroding above a fault-bend fold geometry. A: Cooling ages measured from surface rocks for apatite fission track and (U-Th)/He techniques. B: Basic model of a fault-bend fold. See text for discussion.

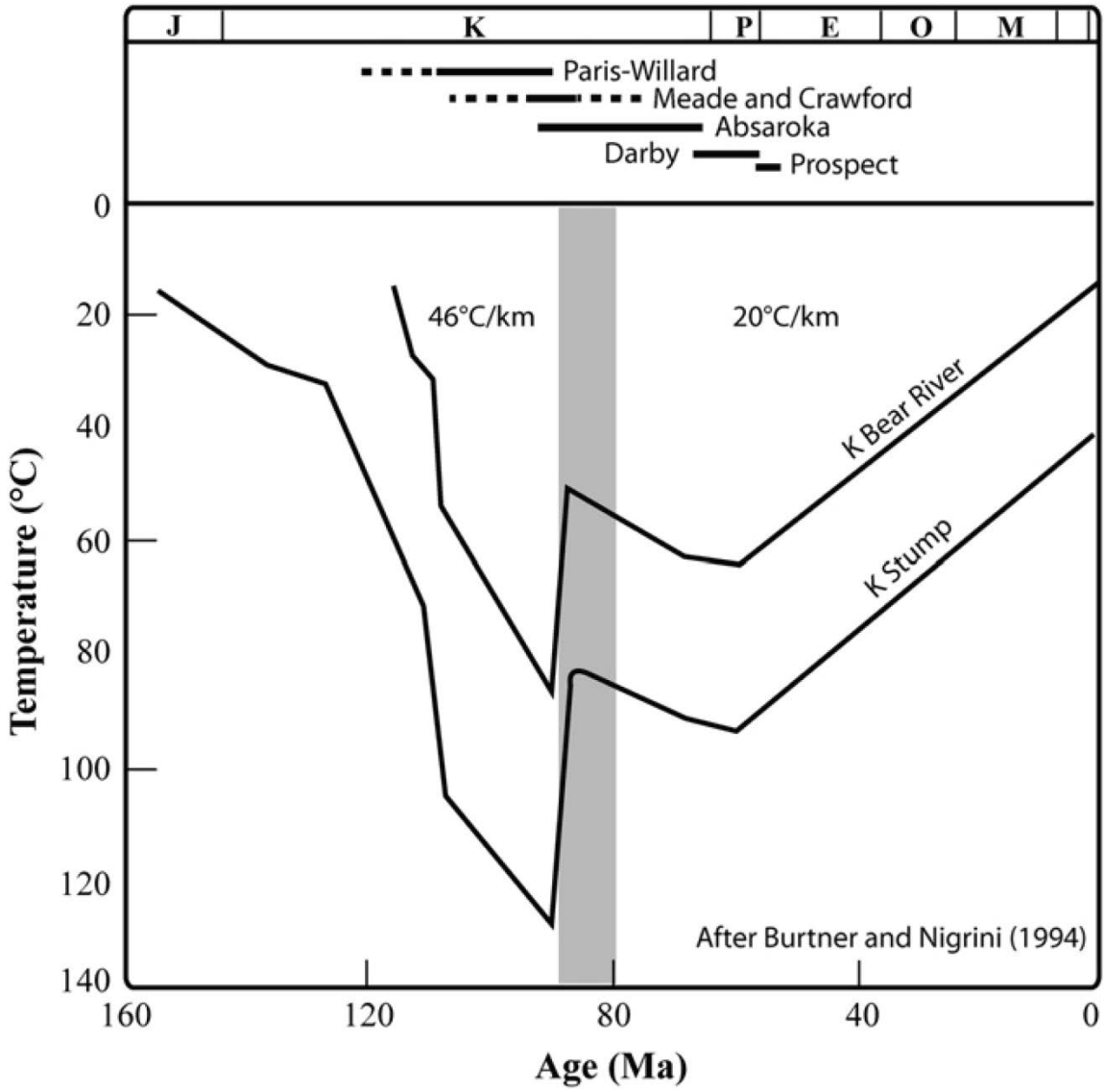

Figure 5: Model from, Burtner and Nigrini, (1994) showing the possible temperature path of samples taken from the Gulf 1 Huff Lake Federal well; see Fig. 6 for location. Samples analyzed for this study may have taken a similar time-temperature path but the actual path of any sample in this study is unknown. Figure is modified from Wiltschko et al. (2009).

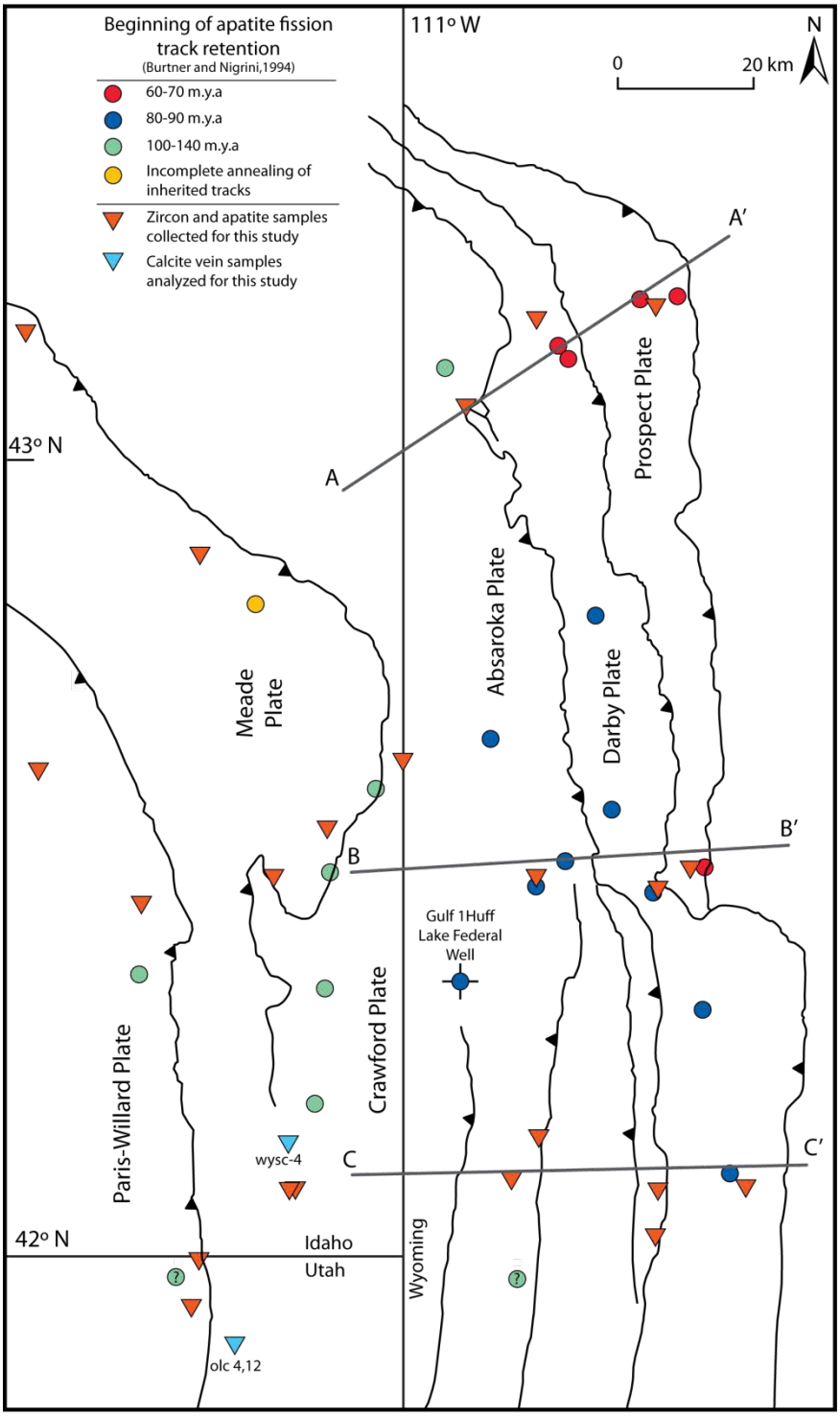
Beginning of apatite fission track retention
(Burtner and Nigrini,1994)
60-70 m.y.a
80-90 m.y.a
100-140 m.y.a
Incomplete annealing of inherited tracks
Zircon and apatite samples collected for this study
Calcite vein samples analyzed for this study
111° W
N
0
20 km
43° N
42° N
A
A′
B
B′
C
C′
Prospect Plate
Absaroka Plate
Darby Plate
Meade Plate
Crawford Plate
Paris-Willard Plate
Gulf 1Huff Lake Federal Well
wysc-4
olc 4,12
Idaho
Utah
Wyoming

Figure 6: Location of cooling events (modified from Burtner and Nigrini, 1994), location of zircon, apatite and calcite vein samples collected for this study and cross-section locations (A-A', B-B', C-C'). The Burtner and Nigrini, (1994) cooling events interpreted from apatite fission track analysis and are inferred to represent cooling associated with uplift and erosion corresponding to motion on major thrust faults.

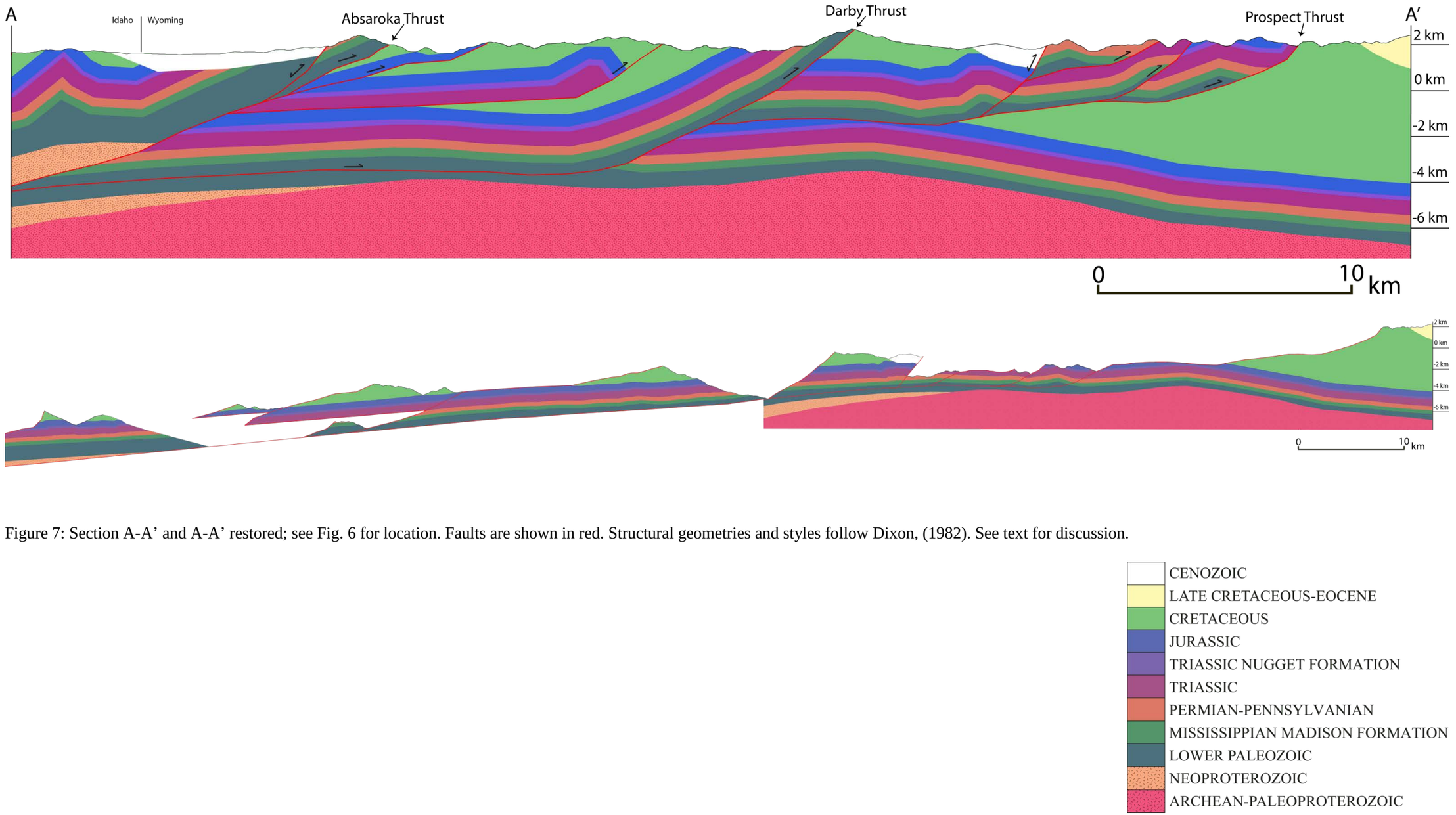

Figure 7: Section A-A’ and A-A’ restored; see Fig. 6 for location. Faults are shown in red. Structural geometries and styles follow Dixon, (1982). See text for discussion.

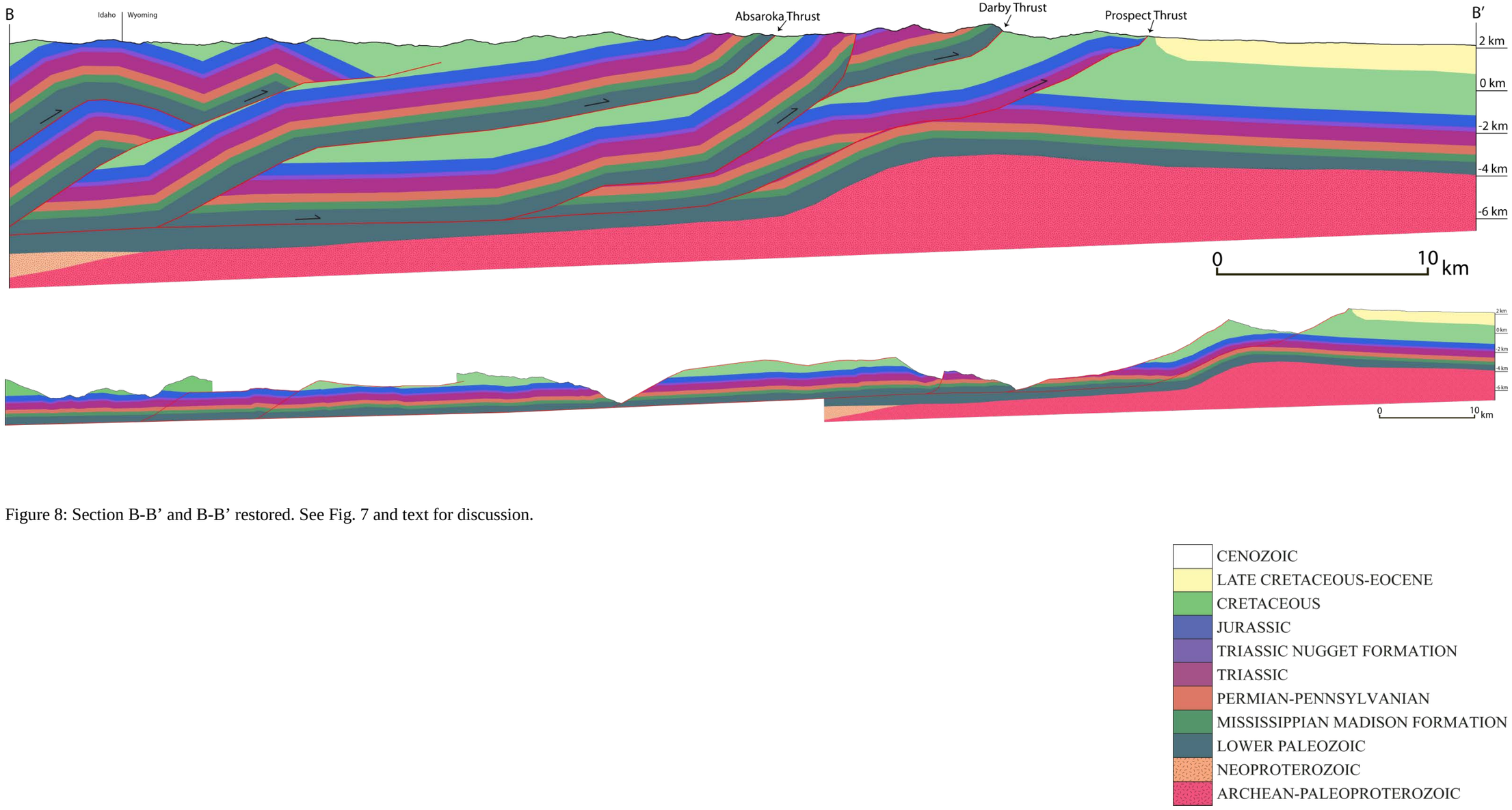

Figure 8: Section B-B’ and B-B’ restored. See Fig. 7 and text for discussion.

Figure 9: Section C-C’ and C-C’ restored. See Fig.7 and text for discussion.

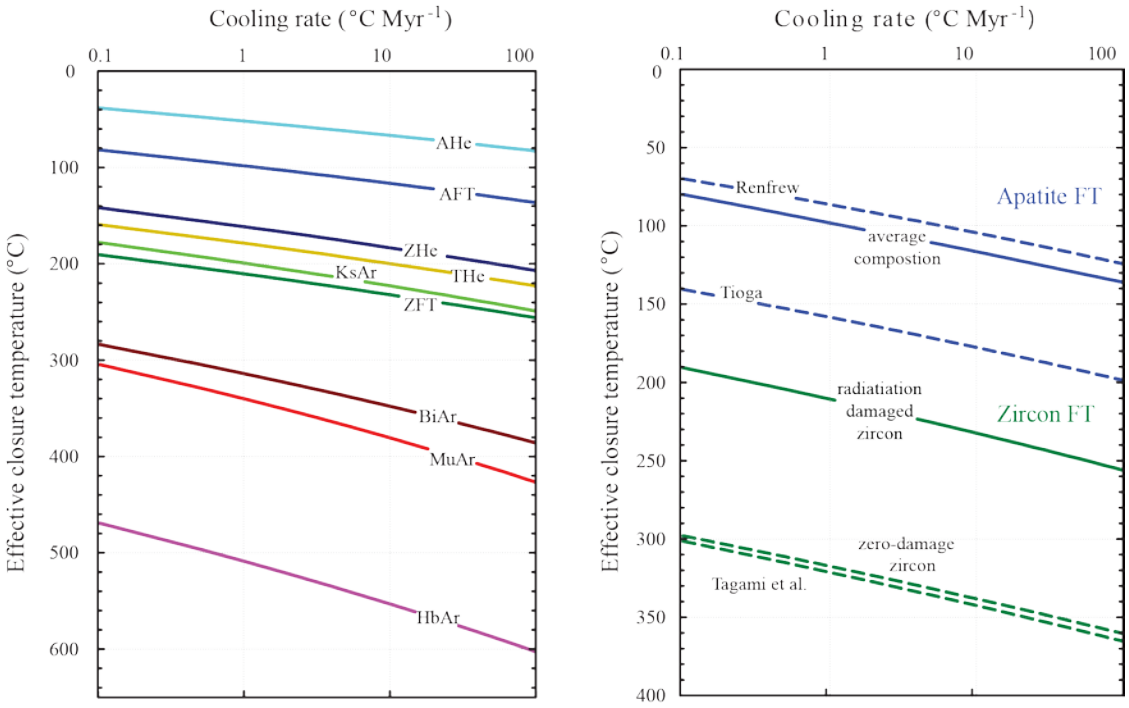

Figure 10: *a*. Diagram (modified from Reiners and Brandon, 2006) showing the effective closure temperature as a function of cooling rate for the common thermochronometers of He, fission track (FT), and Ar. *b.* Diagram showing the effective closure temperature of apatite and zircon as a function of cooling rate. Apatite FT shows the difference in effective closure temperature between low retentivity (Renfrew) and High retentivity (Tioga) apatite (see Ketchum et al. 1999). Zircon FT shows the difference in effective closure temperature between naturally radiation damaged (see Brandon et al. 1998) and zero-damaged zircon (see Tagami et al. 1998).

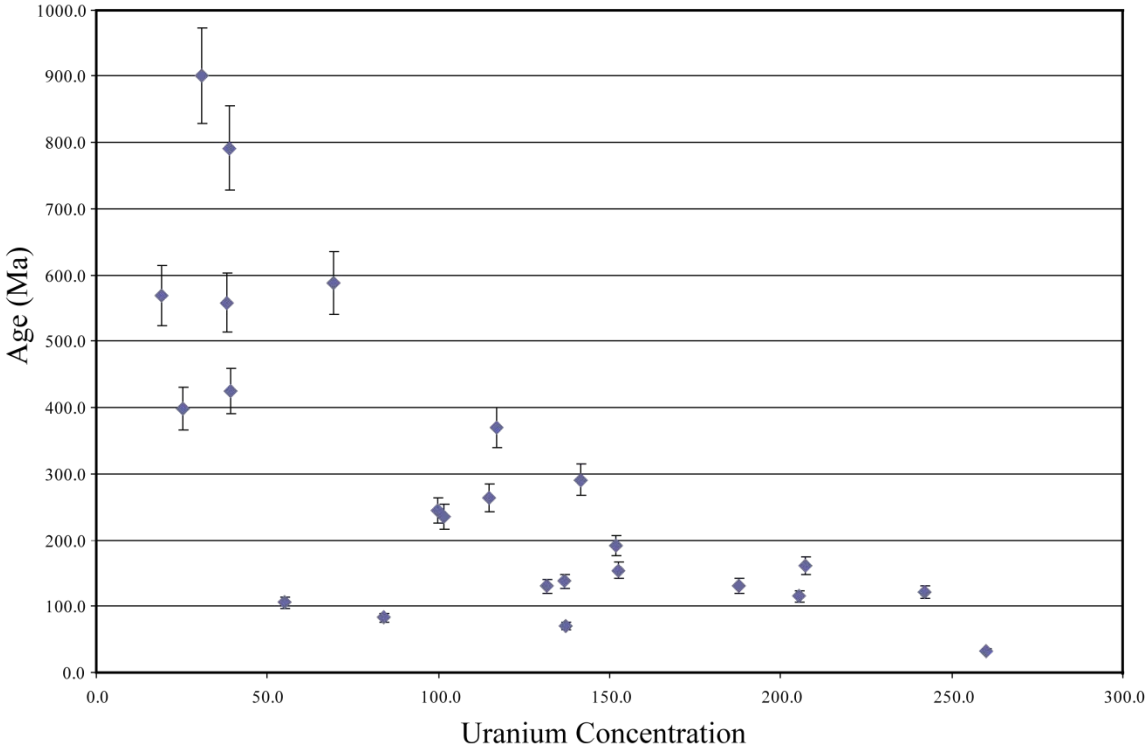

Figure 11: Diagram showing the zircon (U-Th)/He analysis with age (Ma) vs. uranium concentration. Blue diamonds represent an individual analysis and black bars represent the associated error.

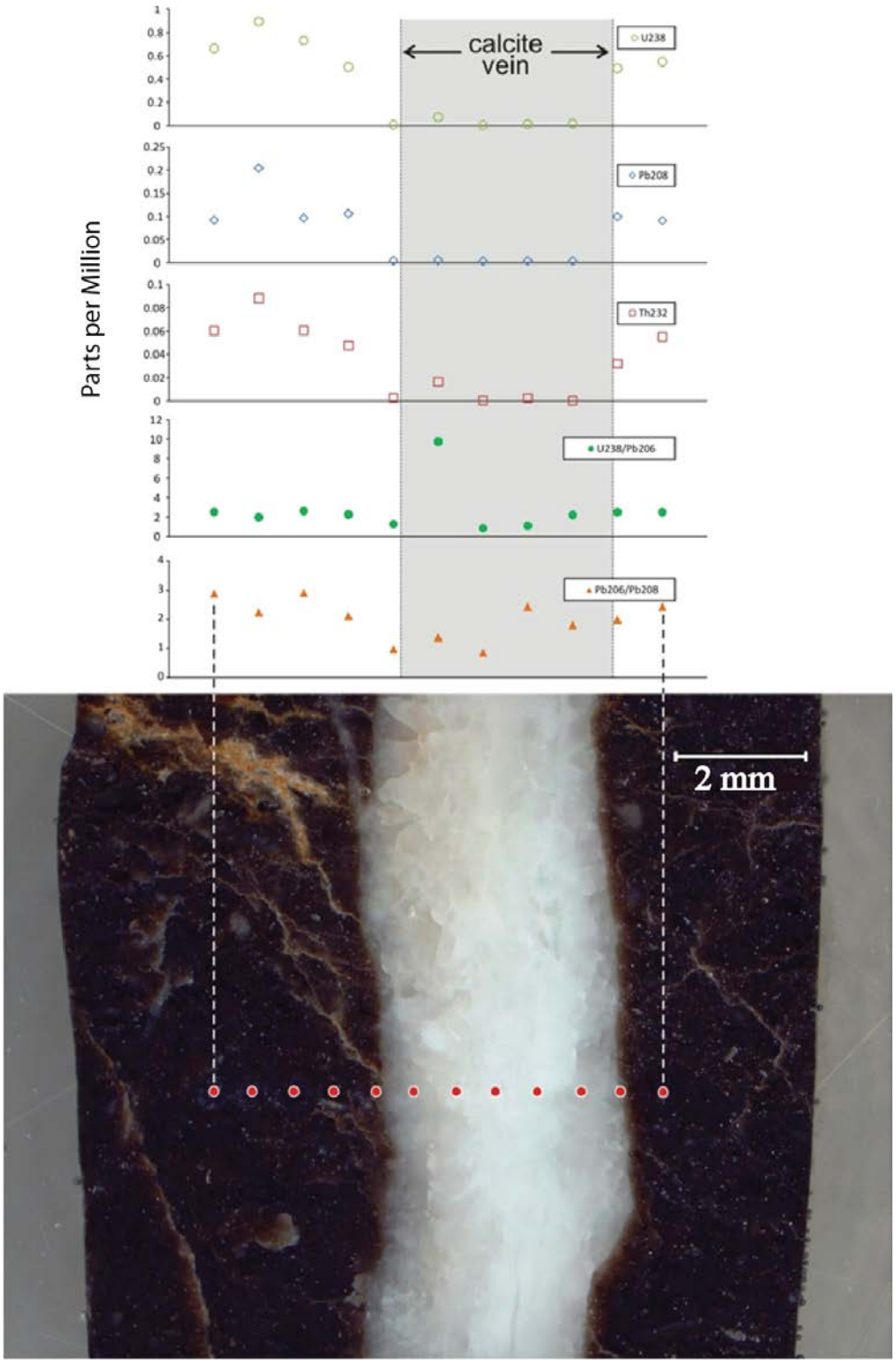
Parts per Million
calcite vein
U238
Pb208
Th232
U238/Pb206
Pb206/Pb208
2 mm

Figure 12: Plot and picture of the LA-ICPMS analysis of vein sample *WYSC-4.* Red dots indicate the single laser spot analysis location. Plot indicates the concentration of a given isotopic component in parts per million. The shaded area represents the vein composition over that of the host material.

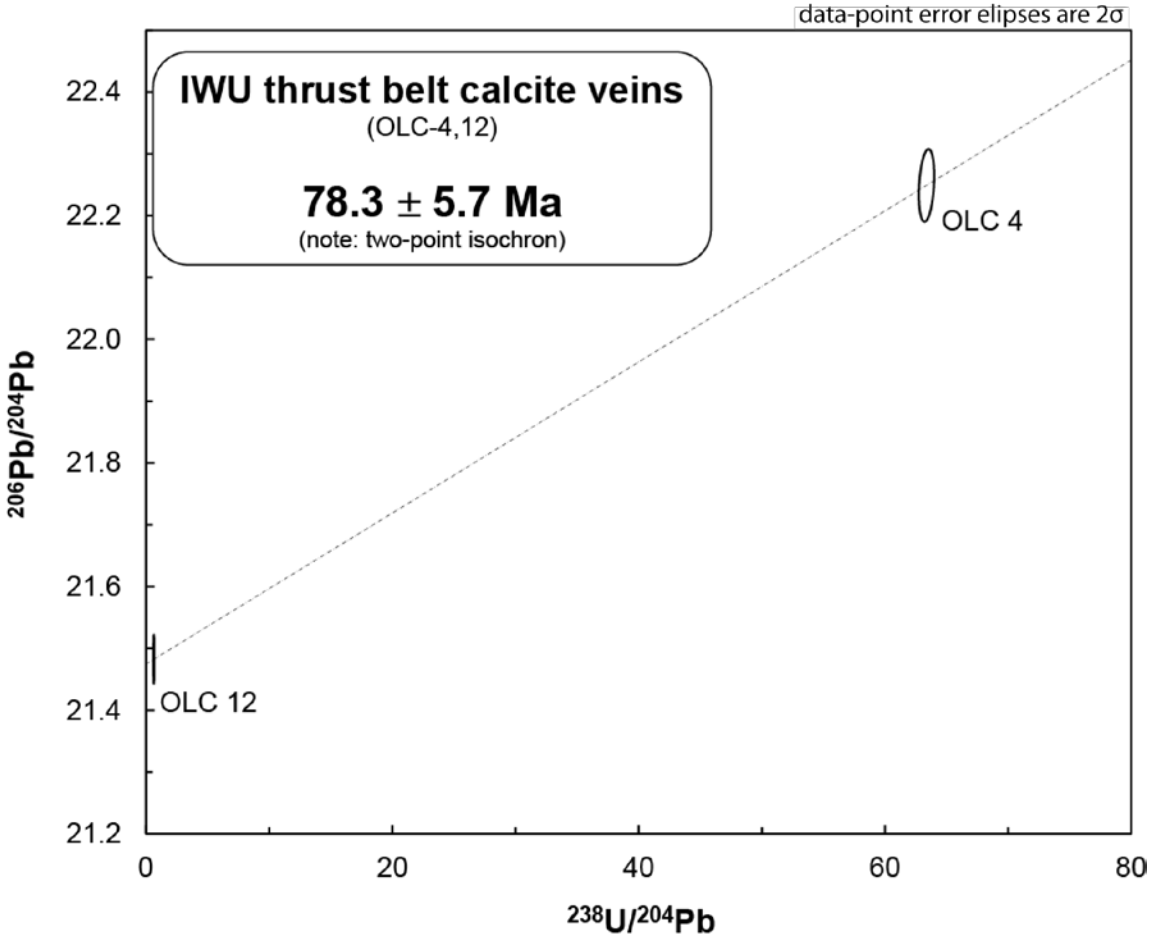

Figure 13: Isochron plot of ID- TIMS analysis of two vein samples OLC 4 and OLC 12. Ellipses indicate the data error at 2σ plotted as ^{206}/Pb^{204}Pb vs. ^{238}U/^{204}Pb.

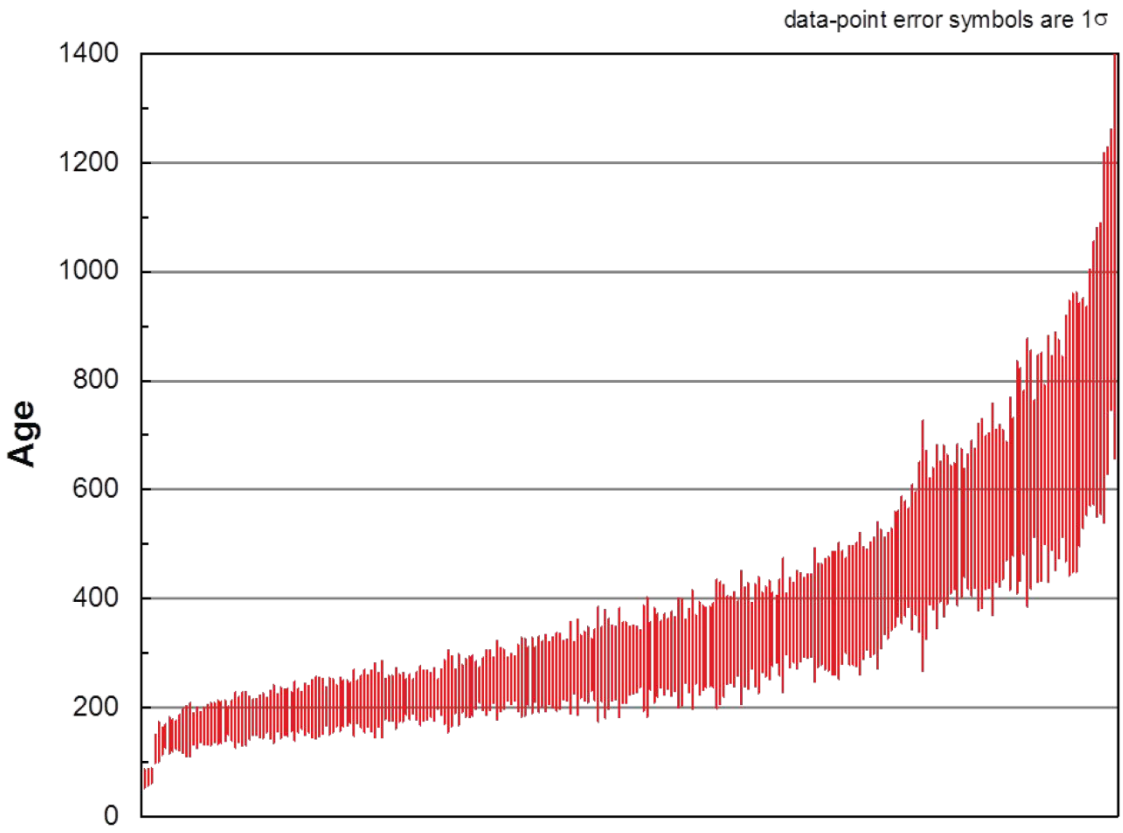

Figure 14: Plot of zircon fission track ages by weighted average of data point errors at 1σ.

Sample No.	No. of Crystals	Track Density (x 10^6 tr cm^{-2})			Age Dispersion	Central Age (Ma)
		ρs (N_s)	ρi (N_i)	ρd (N_d)	($P\chi^2$)	($\pm 1\sigma$)
WYZ 7	4	0.7111 (71)	1.733 (173)	1.616 (5170)	<0.01% (99.7%)	120.9±17.8

Table 1: Analyses by external detector method using 0.5 for the $4\pi/2\pi$ geometry correction factor; ρs is the density of spontaneous tracks and (Ns) the number counted; ρi is the density of induced tracks and (Ni) the number counted; ρd is the density of tracks and (Nd) the number counted using dosimeter glass: IRMM540R with $\zeta 540R$ = 368.1 ±14.9 (apatite); $P\chi 2$ is the probability of obtaining a $\chi 2$ value for v degrees of freedom where v = no. of crystals – 1.

Sample No.	No. of Crystals	Track Density (x 10^6 tr cm^{-2})			Age Dispersion	Age Range (Ma)
		ρ_s (N_s)	ρ_i (N_i)	ρ_d (N_d)	($P\chi^2$)	
WYZ 1	20	13.68 (2722)	1.673 (333)	0.5904 (3779)	<0.01% (>99.9%)	237-356
WYZ 2B	5	22.31 (514)	2.604 (60)	0.5889 (3769)	<0.01% (93.3%)	229-322
WYZ 3	20	17.19 (3642)	2.252 (477)	0.5874 (3759)	24.8% (0.08%)	138-1070
WYZ 5	20	16.54 (4710)	2.184 (622)	0.5859 (3750)	28.2% (<0.01%)	148-678
WYZ 6	20	16.66 (3028)	1.838 (334)	0.5844 (3740)	33.7% (<0.01%)	156-878
WYZ 8	20	26.30 (5184)	1.902 (375)	0.5829 (3731)	26.7% (0.05%)	217-814
WYZ 9	20	21.10 (4618)	1.389 (304)	0.5814 (3721)	9.3% (16.9%)	279-816
WYZ 10	20	31.99 (6163)	2.201 (424)	0.5799 (3711)	3.5% (55.9%)	344-694
WYZ 12	18	15.77 (3059)	2.537 (492)	0.5769 (3692)	18.8% (1.2%)	149-569
WYZ 13	20	15.80 (3499)	1.964 (435)	0.5754 (3682)	23.4% (0.3%)	124-549
WYZ 14	20	18.74 (3813)	2.142 (436)	0.5739 (3673)	36.2% (<0.01%)	153-1004
WYZ 15	16	13.72 (2643)	1.578 (304)	0.5724 (3663)	88.1% (<0.01%)	69-928
WYZ 16B	20	16.51 (3148)	2.218 (423)	0.5709 (3654)	21.6% (0.6%)	173-740
WYZ 18	20	14.24 (3399)	2.086 (498)	0.5694 (3644)	19.7% (0.8%)	136-390
WYZ 22	20	20.24 (4003)	2.953 (584)	5.679 (3634)	18.8% (0.5%)	151-464

Table 2: Analyses by external detector method using 0.5 for the $4\pi/2\pi$ geometry correction factor; ρs is the density of spontaneous tracks and (Ns) the number counted;

ρi is the density of induced tracks and (Ni) the number counted; ρd is the density of tracks and (Nd) the number counted using dosimeter glass: IRMM541 with ζ541 = 121.1±3.5 (zircon); Pχ2 is the probability of obtaining a χ2 value for v degrees of freedom where v = no. of crystals – 1.

Sample No.	Age (Ma)	err., (Ma)	U (ppm)	Th (ppm)	147Sm (ppm)	e (U)	Th/U	He (nmol/g)	mass (ug)	F_T
zWY-10-5	568.3	45.47	16.9	9.9	2.5	19.2	0.59	50.8	18.25	0.83
zWY-10-6	121.6	9.73	122.2	488.3	1462.9	241.9	4.00	125.6	6.86	0.76
zWY-12-1	114.8	9.19	100.8	449.1	226.3	205.4	4.45	100.4	7.96	0.77
zWY-12-2	191.3	15.30	78.6	316.3	80.1	151.8	4.03	120.5	6.36	0.75
zWY-12-4	235.0	18.80	56.8	193.3	64.2	101.6	3.40	102.6	7.58	0.78
zWY-12-5	290.8	23.26	83.8	249.8	61.8	141.6	2.98	169.6	5.74	0.74
zWY-12-6	130.9	10.47	103.5	364.0	71.7	187.6	3.52	102.3	5.59	0.76
zWY-14-1	69.7	5.58	61.9	326.4	64.5	137.3	5.28	40.4	6.21	0.77
zWY-14-2	369.9	29.59	76.3	176.1	26.4	117.0	2.31	175.8	4.41	0.73
zWY-14-3	32.8	2.63	222.3	162.8	22.1	259.9	0.73	35.0	4.83	0.76
zWY-14-4	105.6	8.45	37.7	74.1	16.8	54.9	1.97	24.6	6.72	0.78
zWY-14-5	83.3	6.66	68.4	67.4	13.8	84.0	0.99	28.1	4.92	0.74
zWY-14-6	398.5	31.88	17.3	34.0	45.6	25.4	1.96	44.1	7.70	0.78
zWY-18-1	244.9	19.60	63.7	156.0	38.0	99.8	2.45	102.9	6.40	0.76
zWY-18-2	263.5	21.08	82.6	139.5	18.8	114.9	1.69	132.2	8.94	0.79
zWY-18-3	137.5	11.00	119.4	75.4	30.3	136.9	0.63	79.7	5.99	0.77
zWY-18-4	161.1	12.89	127.5	345.9	29.7	207.3	2.71	137.2	5.56	0.75
zWY-18-6	424.6	33.97	32.5	30.0	10.5	39.4	0.92	76.0	11.64	0.81
zWY-22-1	900.2	72.02	16.2	62.5	57.0	30.9	3.85	118.0	4.89	0.74
zWY-22-2	587.5	47.00	44.2	107.8	36.5	69.2	2.44	173.0	5.86	0.75
zWY-22-3	130.7	10.45	103.1	123.7	25.9	131.7	1.20	71.0	5.49	0.75
zWY-22-4	558.3	44.66	26.5	50.9	13.9	38.2	1.92	93.4	7.21	0.78
zWY-22-5	791.6	63.33	32.0	29.9	8.1	38.9	0.93	139.5	9.13	0.79
zWY-22-6	154.2	12.33	101.7	221.2	30.2	152.7	2.18	99.7	6.66	0.77

Table 3: F_T is a correction factor for loss of alpha ejection from the crystal.

Sample	Olc4	Olc12
Wt (mg)	18.01	24.14
U (ppm)	0.110756	0.000743
Th/U	0.393593	14.28948
Pb (ppm)	0.118507	0.080933
Pb*/Pbc	0.0647	0.07411
Pbc (pg)	2004.847	1819.122
238U/204Pb	63.39138	0.628693
% err	0.802394	5.038927
206Pb/204Pb	22.24885	21.48226
% err	0.216003	0.150699
corr. Coef./8/4-6/4	0.259157	0.027746
235U/204Pb	0.459758	0.00456
% err	0.802394	5.038927
207Pb/204Pb	15.95957	15.94642
% err	0.35647	0.179396
corr. Coef./5/4-7/4	0.155801	0.02294

Table 4

Spot		1	2	3	4	5	6	7	8	9	10	11
SiO2	wt.%	0.431982	0.531194	0.317543	0.195815	0.009793	0.00634	0.005945	0.005595	0.006465	0.0534	0.144729
Mg24	µg/g	1002.978	1157.001	1060.971	870.0742	1100.628	845.0325	513.2966	672.6684	847.6483	986.7793	1004.193
Mn55	µg/g	24.87005	21.72698	24.24239	22.99347	33.06862	36.50524	29.82558	33.83851	38.96518	25.26529	30.75641
Fe57	µg/g	250.6772	436.5938	277.8914	186.6118	4.630288	5.875556	5.101873	4.762376	5.400322	52.39622	242.2283
Sc45	µg/g	0.128078	0.179541	0.106347	0.103027	<0.0059887	0.009675	<0.0076229	<0.013439	<0.0086324	0.027826	0.045467
Rb85	µg/g	0.703119	1.424557	0.510402	0.277805	0.036153	0.033355	0.014102	0.014159	0.01208	0.076348	0.277019
Sr88	µg/g	88.24203	97.68694	96.07884	106.3934	69.72343	84.98594	87.30974	68.64624	49.63486	127.5043	91.22787
Y89	µg/g	2.233422	2.177677	2.417751	3.745923	1.28005	3.104036	1.592541	1.874803	0.303922	2.103856	2.923616
Pb204	µg/g	0.190142	<0.17343	0.19266	<0.15607	<0.16448	<0.14228	<0.14017	<0.15774	<0.14648	<0.1489	0.200923
Pb206	µg/g	0.26568	0.456457	0.28025	0.223701	0.004347	0.007325	0.002757	0.009681	0.00697	0.198346	0.220819
Pb208	µg/g	0.09205	0.203851	0.096476	0.105966	0.004443	0.005312	0.00324	0.003977	0.003862	0.099661	0.090639
Th232	µg/g	0.060281	0.088098	0.060449	0.047428	0.00256	0.016352	0.000306	0.002269	5.99E-05	0.031962	0.055028
U238	µg/g	0.661559	0.892618	0.729595	0.500927	0.00536	0.071373	0.002201	0.010288	0.01523	0.491025	0.546209
U238/Pb206		2.490062	1.955537	2.603373	2.239271	1.233192	9.743367	0.79819	1.062778	2.185229	2.475597	2.47356
Pb206/Pb208		2.886255	2.239163	2.904881	2.111057	0.97834	1.379061	0.850977	2.433961	1.804608	1.990215	2.436246

Table 5

APPENDIX B

APATITE AND ZIRCON FISSION TRACK ANALYSIS

Sample Number		**WYZ1**			Mineral	**Zircon**					
Position (#)		29			Glass (U pp	49.4					
Area of Graticule Squar		6.400E-07			Irradiation	UA-Z2					
No. of Crystals		20			Analyst	SNT					
Zeta Factor ± Error		121.1	3.5								
Rho d (% Relative Error)		5.904E+05	1.63								
N d		3779									
N s	N i	N g	Rho s	Rho i	Rho s / Rho	U ppm	Age (Ma)	Age error	50% Age	"+95%"	"-95%"
83	10	12	1.081E+07	1.302E+06	8.3000	108.9	**290.09**	**97.58**	**302.15**	**309.44**	**150.42**
67	8	8	1.309E+07	1.563E+06	8.3750	130.7	**292.65**	**109.90**	**307.94**	**376.24**	**165.98**
105	11	12	1.367E+07	1.432E+06	9.5455	119.8	**332.51**	**105.95**	**344.69**	**323.89**	**164.13**
86	11	8	1.680E+07	2.148E+06	7.8182	179.8	**273.60**	**88.08**	**284.05**	**271.99**	**137.08**
120	16	15	1.250E+07	1.667E+06	7.5000	139.5	**262.69**	**70.45**	**269.60**	**197.22**	**112.99**
188	22	21	1.399E+07	1.637E+06	8.5455	137.0	**298.47**	**67.98**	**303.99**	**176.81**	**110.99**
145	20	16	1.416E+07	1.953E+06	7.2500	163.4	**254.10**	**61.19**	**259.48**	**163.25**	**99.69**
143	18	18	1.241E+07	1.563E+06	7.9444	130.7	**277.93**	**70.12**	**284.33**	**190.64**	**113.23**
155	23	16	1.514E+07	2.246E+06	6.7391	187.9	**236.52**	**53.43**	**240.94**	**138.97**	**87.91**
82	9	12	1.068E+07	1.172E+06	9.1111	98.1	**317.75**	**112.07**	**332.19**	**366.12**	**170.77**
121	16	20	9.453E+06	1.250E+06	7.5625	104.6	**264.83**	**71.00**	**271.79**	**198.67**	**113.84**
102	14	8	1.992E+07	2.734E+06	7.2857	228.8	**255.33**	**73.26**	**263.08**	**212.21**	**116.43**
161	20	16	1.572E+07	1.953E+06	8.0500	163.4	**281.54**	**67.40**	**287.35**	**179.10**	**109.55**
144	17	10	2.250E+07	2.656E+06	8.4706	222.3	**295.92**	**76.52**	**303.04**	**210.16**	**122.91**
86	10	12	1.120E+07	1.302E+06	8.6000	108.9	**300.33**	**100.84**	**312.73**	**319.18**	**155.31**
118	16	16	1.152E+07	1.563E+06	7.3750	130.7	**258.40**	**69.37**	**265.22**	**194.32**	**111.30**
104	13	12	1.354E+07	1.693E+06	8.0000	141.6	**279.83**	**82.84**	**288.79**	**243.69**	**130.62**
278	32	24	1.810E+07	2.083E+06	8.6875	174.3	**303.32**	**57.51**	**307.15**	**139.93**	**95.70**
215	21	30	1.120E+07	1.094E+06	10.2381	91.5	**355.99**	**82.24**	**362.64**	**214.21**	**133.33**
219	26	25	1.369E+07	1.625E+06	8.4231	136.0	**294.29**	**61.82**	**298.91**	**155.97**	**101.92**
**********	**********	**********	**********	**********	**********	**********	**********	**********	**********	**********	**********
2722	333	311	1.368E+07	1.673E+06	8.1742	140.0	**285.79**	**19.11**	**286.14**	**34.19**	**30.58**
Pooled Ratio		8.1742	±	0.5465							
Mean Ratio		8.1911	±	0.1864							
Pooled Age		285.79	±	19.11	1 S.E.						
Mean Crystal Age		286.36	±	6.66	1 S.E.						
Binomial Age		286.14	+	34.19	"+95%"						
			-	30.58	"-95%"						
Central Age		**285.79**	**±**	**19.11**							
Age Dispersion		**0.00**	%								
Chi-squared		**3.071**	with	19	degrees of freedom						
P (Chi-Sq)		**100.00**	**%**								

Sample Number		**WYZ2B**			Mineral	**Zircon**					
Position (#)		30			Glass (U pp	49.4					
Area of Graticule Squar		6.400E-07			Irradiation	UA-Z2					
No. of Crystals		5			Analyst	SNT					
Zeta Factor ± Error		121.1	3.5								
Rho d (% Relative Error)		5.889E+05	1.63								
N d		3769									
N s	N i	N g	Rho s	Rho i	Rho s / Rho	U ppm	Age (Ma)	Age error	50% Age	"+95%"	"-95%"
102	11	10	1.594E+07	1.719E+06	9.2727	144.2	**322.45**	**102.89**	**334.32**	**315.04**	**159.50**
73	8	4	2.852E+07	3.125E+06	9.1250	262.1	**317.43**	**118.69**	**333.72**	**404.32**	**178.88**
172	19	10	2.688E+07	2.969E+06	9.0526	249.0	**314.98**	**76.86**	**321.66**	**205.47**	**124.20**
72	11	6	1.875E+07	2.865E+06	6.5455	240.3	**229.27**	**74.61**	**238.41**	**232.26**	**116.59**
95	11	6	2.474E+07	2.865E+06	8.6364	240.3	**300.83**	**96.33**	**312.07**	**296.05**	**149.58**
**********	**********	**********	**********	**********	**********	**********	**********	**********	**********	**********	**********
514	60	36	2.231E+07	2.604E+06	8.5667	218.5	**298.45**	**41.90**	**300.46**	**93.36**	**71.13**
Pooled Ratio		8.5667	±	1.2028							
Mean Ratio		8.5264	±	0.5064							
Pooled Age		298.45	±	41.90	1 S.E.						
Mean Crystal Age		297.08	±	18.03	1 S.E.						
Binomial Age		300.46	+	93.36	"+95%"						
			-	71.13	"-95%"						
Central Age		**298.45**	**±**	**41.90**							
Age Dispersion		**0.00**	%								
Chi-squared		**0.839**	with	4	degrees of freedom						
P (Chi-Sq)		**93.31**	**%**								

Sample Number		**WYZ3**			Mineral	**Zircon**					
Position (#)		31			Glass (U pp	49.4					
Area of Graticule Squar		6.400E-07			Irradiation	UA-Z2					
No. of Crystals		20			Analyst	SNT					
Zeta Factor ± Error		121.1	3.5								
Rho d (% Relative Error)		5.874E+05	1.63								
N d		3759									
N s	N i	N g	Rho s	Rho i	Rho s / Rho	U ppm	Age (Ma)	Age error	50% Age	"+95%"	"-95%"
149	38	15	1.552E+07	3.958E+06	3.9211	332.9	**137.97**	**25.49**	**139.80**	**61.78**	**43.41**
231	27	12	3.008E+07	3.516E+06	8.5556	295.7	**297.33**	**61.27**	**301.80**	**153.49**	**101.18**
351	56	40	1.371E+07	2.188E+06	6.2679	184.0	**219.16**	**32.36**	**220.86**	**73.44**	**55.25**
320	40	28	1.786E+07	2.232E+06	8.0000	187.7	**278.44**	**47.60**	**281.29**	**112.29**	**80.07**
144	19	12	1.875E+07	2.474E+06	7.5789	208.1	**264.08**	**65.05**	**269.90**	**175.16**	**105.53**
208	27	20	1.625E+07	2.109E+06	7.7037	177.4	**268.34**	**55.61**	**272.46**	**139.83**	**92.04**
135	27	20	1.055E+07	2.109E+06	5.0000	177.4	**175.43**	**37.44**	**178.45**	**95.39**	**62.51**
73	12	9	1.267E+07	2.083E+06	6.0833	175.2	**212.81**	**66.67**	**220.72**	**202.88**	**105.09**
228	35	20	1.781E+07	2.734E+06	6.5143	230.0	**227.63**	**42.01**	**230.43**	**101.76**	**70.62**
165	22	15	1.719E+07	2.292E+06	7.5000	192.7	**261.38**	**59.96**	**266.36**	**156.74**	**98.18**
229	7	15	2.385E+07	7.292E+05	32.7143	61.3	**1069.68**	**411.97**	**1121.30**	**1291.72**	**588.28**
150	16	10	2.344E+07	2.500E+06	9.3750	210.2	**325.10**	**86.18**	**333.26**	**238.98**	**137.53**
308	43	32	1.504E+07	2.100E+06	7.1628	176.6	**249.85**	**41.51**	**252.30**	**97.25**	**70.17**
158	16	7	3.527E+07	3.571E+06	9.8750	300.4	**341.99**	**90.44**	**350.48**	**250.18**	**144.15**
110	15	9	1.910E+07	2.604E+06	7.3333	219.0	**255.69**	**70.89**	**262.91**	**201.76**	**113.22**
138	17	21	1.027E+07	1.265E+06	8.1176	106.4	**282.44**	**73.20**	**289.31**	**201.44**	**117.70**
130	17	8	2.539E+07	3.320E+06	7.6471	279.2	**266.40**	**69.27**	**272.96**	**191.09**	**111.53**
131	9	12	1.706E+07	1.172E+06	14.5556	98.6	**497.96**	**172.39**	**518.76**	**545.70**	**259.53**
138	17	12	1.797E+07	2.214E+06	8.1176	186.2	**282.44**	**73.20**	**289.31**	**201.44**	**117.70**
146	17	14	1.629E+07	1.897E+06	8.5882	159.6	**298.44**	**77.12**	**305.61**	**211.72**	**123.84**
**********	**********	**********	**********	**********	**********	**********	**********	**********	**********	**********	**********
3642	477	331	1.719E+07	2.252E+06	7.6352	189.4	**266.00**	**15.67**	**266.23**	**26.41**	**24.06**
Pooled Ratio		7.6352	±	0.4499							
Mean Ratio		9.0306	±	1.3327							
Pooled Age		266.00	±	15.67	1 S.E.						
Mean Crystal Age		313.45	±	47.23	1 S.E.						
Binomial Age		266.23	+	26.41	"+95%"						
			-	24.06	"-95%"						
Central Age		**267.08**	**±**	**21.90**							
Age Dispersion		**24.75**	%								
Chi-squared		**44.443**	with	19	degrees of freedom						
P (Chi-Sq)		**0.08**	**%**								

Sample Number		**WYZ5**			Mineral	**Zircon**					
Position (#)		32			Glass (U pp	49.4					
Area of Graticule Squar		6.400E-07			Irradiation	UA-Z2					
No. of Crystals		20			Analyst	SNT					
Zeta Factor ± Error		121.1	3.5								
Rho d (% Relative Error)		5.859E+05	1.63								
N d		3750									
N s	N i	N g	Rho s	Rho i	Rho s / Rho	U ppm	Age (Ma)	Age error	50% Age	"+95%"	"-95%"
195	14	12	2.539E+07	1.823E+06	13.9286	153.7	**476.11**	**132.68**	**488.85**	**371.75**	**207.56**
122	21	21	9.077E+06	1.563E+06	5.8095	131.7	**202.87**	**48.40**	**207.19**	**128.82**	**79.46**
178	19	8	3.477E+07	3.711E+06	9.3684	312.9	**324.07**	**78.95**	**330.90**	**210.78**	**127.48**
154	19	14	1.719E+07	2.121E+06	8.1053	178.8	**281.32**	**69.04**	**287.42**	**185.43**	**111.84**
187	30	20	1.461E+07	2.344E+06	6.2333	197.6	**217.43**	**43.37**	**220.59**	**107.84**	**72.47**
567	88	50	1.772E+07	2.750E+06	6.4432	231.9	**224.62**	**26.79**	**225.72**	**57.47**	**45.92**
209	30	20	1.633E+07	2.344E+06	6.9667	197.6	**242.53**	**48.03**	**245.97**	**119.03**	**80.08**
237	37	25	1.481E+07	2.313E+06	6.4054	195.0	**223.33**	**40.17**	**225.94**	**96.52**	**67.69**
143	15	8	2.793E+07	2.930E+06	9.5333	247.0	**329.63**	**90.13**	**338.43**	**253.63**	**143.11**
254	60	30	1.323E+07	3.125E+06	4.2333	263.5	**148.46**	**21.87**	**149.67**	**49.68**	**37.69**
189	21	12	2.461E+07	2.734E+06	9.0000	230.5	**311.63**	**72.42**	**317.61**	**189.76**	**117.79**
239	27	18	2.075E+07	2.344E+06	8.8519	197.6	**306.62**	**63.08**	**311.20**	**157.83**	**104.09**
159	22	18	1.380E+07	1.910E+06	7.2273	161.0	**251.43**	**57.80**	**256.26**	**151.31**	**94.72**
363	18	25	2.269E+07	1.125E+06	20.1667	94.9	**678.45**	**165.37**	**691.75**	**426.34**	**260.24**
308	29	30	1.604E+07	1.510E+06	10.6207	127.4	**366.18**	**72.16**	**371.09**	**177.04**	**118.97**
472	68	60	1.229E+07	1.771E+06	6.9412	149.3	**241.66**	**32.36**	**243.16**	**71.44**	**55.29**
126	23	14	1.406E+07	2.567E+06	5.4783	216.4	**191.48**	**43.88**	**195.25**	**114.90**	**72.51**
192	35	20	1.500E+07	2.734E+06	5.4857	230.5	**191.73**	**35.81**	**194.21**	**87.17**	**60.40**
180	11	10	2.813E+07	1.719E+06	16.3636	144.9	**555.85**	**173.62**	**574.40**	**512.38**	**265.15**
236	35	30	1.229E+07	1.823E+06	6.7429	153.7	**234.88**	**43.25**	**237.75**	**104.67**	**72.66**
**********	**********	**********	**********	**********	**********	**********	**********	**********	**********	**********	**********
4710	622	445	1.654E+07	2.184E+06	7.5723	184.1	**263.19**	**14.23**	**263.37**	**22.72**	**20.95**
Pooled Ratio		7.5723	±	0.4093							
Mean Ratio		8.6953	±	0.8891							
Pooled Age		263.19	±	14.23	1 S.E.						
Mean Crystal Age		301.32	±	31.47	1 S.E.						
Binomial Age		263.37	+	22.72	"+95%"						
			-	20.95	"-95%"						
Central Age		**265.22**	**±**	**22.35**							
Age Dispersion		**28.16**	%								
Chi-squared		**63.346**	with	19	degrees of freedom						
P (Chi-Sq)		**0.00**	**%**								

Sample Number		**WYZ6**			Mineral	**Zircon**					
Position (#)		33			Glass (U pp	49.4					
Area of Graticule Squar		6.400E-07			Irradiation	UA-Z2					
No. of Crystals		20			Analyst	SNT					
Zeta Factor ± Error		121.1	3.5								
Rho d (% Relative Error)		5.844E+05	1.64								
N d		3740									
N s	N i	N g	Rho s	Rho i	Rho s / Rho	U ppm	Age (Ma)	Age error	50% Age	"+95%"	"-95%"
68	11	10	1.063E+07	1.719E+06	6.1818	145.3	**215.12**	**70.27**	**223.82**	**219.34**	**109.96**
221	14	16	2.158E+07	1.367E+06	15.7857	115.6	**535.70**	**148.70**	**549.75**	**413.17**	**231.80**
186	7	10	2.906E+07	1.094E+06	26.5714	92.5	**877.69**	**339.17**	**921.26**	**1097.84**	**488.73**
151	10	12	1.966E+07	1.302E+06	15.1000	110.1	**513.33**	**168.48**	**532.46**	**514.64**	**255.82**
59	13	6	1.536E+07	3.385E+06	4.5385	286.2	**158.63**	**48.89**	**164.54**	**147.00**	**78.05**
81	15	8	1.582E+07	2.930E+06	5.4000	247.6	**188.30**	**53.30**	**194.06**	**153.43**	**85.69**
189	16	20	1.477E+07	1.250E+06	11.8125	105.7	**405.00**	**106.30**	**414.72**	**291.44**	**168.70**
98	17	12	1.276E+07	2.214E+06	5.7647	187.1	**200.83**	**53.18**	**206.14**	**148.23**	**86.14**
99	15	12	1.289E+07	1.953E+06	6.6000	165.1	**229.41**	**64.02**	**236.06**	**182.99**	**102.49**
110	19	14	1.228E+07	2.121E+06	5.7895	179.3	**201.68**	**50.55**	**206.43**	**137.41**	**82.48**
278	26	25	1.738E+07	1.625E+06	10.6923	137.4	**367.66**	**76.38**	**373.16**	**190.90**	**125.23**
175	22	12	2.279E+07	2.865E+06	7.9545	242.1	**275.50**	**62.99**	**280.68**	**164.34**	**103.02**
169	21	16	1.650E+07	2.051E+06	8.0476	173.4	**278.66**	**65.14**	**284.13**	**171.44**	**106.21**
249	36	20	1.945E+07	2.813E+06	6.9167	237.7	**240.22**	**43.57**	**243.05**	**104.90**	**73.23**
189	18	20	1.477E+07	1.406E+06	10.5000	118.9	**361.23**	**89.91**	**369.10**	**241.58**	**144.27**
248	10	20	1.938E+07	7.813E+05	24.8000	66.0	**822.75**	**266.77**	**851.30**	**777.29**	**398.36**
85	19	8	1.660E+07	3.711E+06	4.4737	313.7	**156.39**	**40.02**	**160.37**	**109.65**	**65.64**
111	13	12	1.445E+07	1.693E+06	8.5385	143.1	**295.27**	**87.11**	**304.60**	**255.59**	**137.17**
161	18	21	1.198E+07	1.339E+06	8.9444	113.2	**308.98**	**77.47**	**315.92**	**209.69**	**124.79**
101	14	10	1.578E+07	2.188E+06	7.2143	184.9	**250.36**	**71.88**	**257.97**	**208.35**	**114.26**
**********	**********	**********	**********	**********	**********	**********	**********	**********	**********	**********	**********
3028	334	284	1.666E+07	1.838E+06	9.0659	155.3	**313.07**	**20.83**	**313.45**	**37.11**	**33.20**
Pooled Ratio		9.0659	±	0.6032							
Mean Ratio		10.0813	±	1.3849							
Pooled Age		313.07	±	20.83	1 S.E.						
Mean Crystal Age		347.21	±	48.82	1 S.E.						
Binomial Age		313.45	+	37.11	"+95%"						
			-	33.20	"-95%"						
Central Age		**292.62**	**±**	**29.59**							
Age Dispersion		**33.69**	%								
Chi-squared		**57.383**	with	19	degrees of freedom						
P (Chi-Sq)		**0.00**	**%**								

Sample Number		**WYZ 7**			Mineral	**Apatite**							
Position (#)		4			Glass (U p	15							
Area of Graticule Squa		6.400E-07			Irradiation	UA-A6							
No. of Crystals		4			Analyst	SNT							
Zeta Factor ± Error		368.1	14.9										
Rho d (% Relative Erro		########	1.39										
N d		5170											
N s	N i	N g	Dpar	Dper	Rho s	Rho i	Rho s / Rho	U ppm	Age (Ma)	Age error	50% Age	"+95%"	"-95%"
20	49	40	2.38	0.55	########	########	0.4082	17.8	**120.27**	**32.33**	125.09	79.66	57.09
11	28	49	2.45	0.68	########	########	0.3929	8.3	**115.80**	**41.50**	124.23	113.44	71.95
11	25	27	2.69	0.63	########	########	0.4400	13.4	**129.56**	**47.20**	139.18	130.81	81.32
29	71	40	2.68	0.80	########	########	0.4085	25.7	**120.35**	**27.02**	123.67	63.17	48.09
**********	**********	**********	**********	**********	**********	**********	**********	**********	**********	**********	**********	**********	**********
71	173	156	2.55	0.67	########	########	0.4104	16.1	**120.92**	**17.81**	122.28	37.52	31.66
Pooled Ratio		0.4104	±	0.0605									
Mean Ratio		0.4124	±	0.0099									
Pooled Age		120.92	±	17.81	1 S.E.								
Mean Crystal Age		121.50	±	2.95	1 S.E.								
Binomial Age		122.28	+	37.52	"+95%"								
			-	31.66	"-95%"								
Central Age		**120.92**	**±**	**17.81**									
Age Dispersion		**0.00**	%										
Chi-squared		**0.053**	with	3	degrees of freedom								
P (Chi-Sq)		**99.68**	**%**										

Sample Number		**WYZ8**			Mineral	**Zircon**					
Position (#)		34			Glass (U pp	49.4					
Area of Graticule Squar		6.400E-07			Irradiation	UA-Z2					
No. of Crystals		20			Analyst	SNT					
Zeta Factor ± Error		121.1	3.5								
Rho d (% Relative Error)		5.829E+05	1.64								
N d		3731									
N s	N i	N g	Rho s	Rho i	Rho s / Rho	U ppm	Age (Ma)	Age error	50% Age	"+95%"	"-95%"
532	28	36	2.309E+07	1.215E+06	19.0000	103.0	**637.96**	**125.50**	**646.03**	**299.99**	**202.97**
114	10	6	2.969E+07	2.604E+06	11.4000	220.7	**390.30**	**129.37**	**405.55**	**403.17**	**197.94**
152	14	8	2.969E+07	2.734E+06	10.8571	231.7	**372.24**	**104.70**	**382.64**	**297.79**	**164.88**
404	21	21	3.006E+07	1.563E+06	19.2381	132.4	**645.57**	**146.07**	**656.47**	**366.86**	**232.53**
237	11	12	3.086E+07	1.432E+06	21.5455	121.4	**718.83**	**222.99**	**741.89**	**642.37**	**337.50**
324	20	15	3.375E+07	2.083E+06	16.2000	176.6	**547.82**	**127.53**	**557.79**	**327.22**	**203.58**
449	25	25	2.806E+07	1.563E+06	17.9600	132.4	**604.63**	**125.86**	**613.27**	**307.81**	**202.81**
244	21	15	2.542E+07	2.188E+06	11.6190	185.4	**397.57**	**91.37**	**404.84**	**236.70**	**147.70**
183	17	12	2.383E+07	2.214E+06	10.7647	187.6	**369.16**	**94.40**	**377.64**	**256.56**	**150.81**
206	33	20	1.609E+07	2.578E+06	6.2424	218.5	**216.64**	**41.25**	**219.51**	**101.00**	**69.24**
306	22	20	2.391E+07	1.719E+06	13.9091	145.7	**473.12**	**105.61**	**481.12**	**268.55**	**170.35**
169	8	10	2.641E+07	1.250E+06	21.1250	105.9	**705.54**	**256.36**	**737.03**	**815.30**	**377.39**
176	9	8	3.438E+07	1.758E+06	19.5556	149.0	**655.70**	**225.14**	**681.90**	**694.60**	**335.96**
295	12	15	3.073E+07	1.250E+06	24.5833	105.9	**814.03**	**241.24**	**837.50**	**670.07**	**365.90**
284	20	20	2.219E+07	1.563E+06	14.2000	132.4	**482.66**	**112.81**	**491.62**	**291.84**	**180.80**
280	27	15	2.917E+07	2.813E+06	10.3704	238.4	**356.00**	**72.71**	**361.16**	**180.79**	**119.53**
180	20	12	2.344E+07	2.604E+06	9.0000	220.7	**310.07**	**73.81**	**316.33**	**195.33**	**119.69**
249	18	15	2.594E+07	1.875E+06	13.8333	158.9	**470.64**	**115.93**	**480.40**	**306.94**	**184.69**
290	29	15	3.021E+07	3.021E+06	10.0000	256.0	**343.62**	**67.89**	**348.28**	**167.03**	**112.11**
110	10	8	2.148E+07	1.953E+06	11.0000	165.5	**377.00**	**125.15**	**391.82**	**390.87**	**191.64**
**********	**********	**********	**********	**********	**********	**********	**********	**********	**********	**********	**********
5184	375	308	2.630E+07	1.902E+06	13.8240	161.2	**470.33**	**29.61**	**470.79**	**50.80**	**45.83**
Pooled Ratio		13.8240	±	0.8702							
Mean Ratio		14.6202	±	1.1145							
Pooled Age		470.33	±	29.61	1 S.E.						
Mean Crystal Age		496.40	±	39.22	1 S.E.						
Binomial Age		470.79	+	50.80	"+95%"						
			-	45.83	"-95%"						
Central Age		**455.99**	**±**	**39.99**							
Age Dispersion		**26.74**	%								
Chi-squared		**45.790**	with	19	degrees of freedom						
P (Chi-Sq)		**0.05**	**%**								

Sample Number		**WYZ9**			Mineral	**Zircon**					
Position (#)		35			Glass (U pp	49.4					
Area of Graticule Squar		6.400E-07			Irradiation	UA-Z2					
No. of Crystals		20			Analyst	SNT					
Zeta Factor ± Error		121.1	3.5								
Rho d (% Relative Error)		5.814E+05	1.64								
N d		3721									
N s	N i	N g	Rho s	Rho i	Rho s / Rho	U ppm	Age (Ma)	Age error	50% Age	"+95%"	"-95%"
247	10	12	3.216E+07	1.302E+06	24.7000	110.6	**815.68**	**264.50**	**844.01**	**771.48**	**395.10**
169	8	16	1.650E+07	7.813E+05	21.1250	66.4	**703.82**	**255.73**	**735.24**	**813.54**	**376.49**
363	23	30	1.891E+07	1.198E+06	15.7826	101.8	**532.96**	**115.96**	**541.41**	**290.29**	**186.81**
159	14	10	2.484E+07	2.188E+06	11.3571	185.9	**387.91**	**108.91**	**398.65**	**309.04**	**171.32**
171	9	12	2.227E+07	1.172E+06	19.0000	99.6	**636.40**	**218.67**	**661.94**	**676.71**	**326.63**
249	22	16	2.432E+07	2.148E+06	11.3182	182.5	**386.61**	**86.94**	**393.39**	**223.52**	**141.04**
333	14	18	2.891E+07	1.215E+06	23.7857	103.3	**787.26**	**216.37**	**806.74**	**580.98**	**332.56**
208	10	12	2.708E+07	1.302E+06	20.8000	110.6	**693.55**	**225.71**	**718.21**	**670.47**	**339.30**
159	14	10	2.484E+07	2.188E+06	11.3571	185.9	**387.91**	**108.91**	**398.65**	**309.04**	**171.32**
154	19	12	2.005E+07	2.474E+06	8.1053	210.2	**279.20**	**68.52**	**285.27**	**184.09**	**111.01**
167	9	30	8.698E+06	4.688E+05	18.5556	39.8	**622.21**	**213.92**	**647.26**	**663.52**	**319.78**
267	20	16	2.607E+07	1.953E+06	13.3500	166.0	**453.63**	**106.24**	**462.14**	**275.87**	**170.59**
271	17	16	2.646E+07	1.660E+06	15.9412	141.1	**538.09**	**135.72**	**549.67**	**360.55**	**214.50**
281	17	20	2.195E+07	1.328E+06	16.5294	112.8	**557.12**	**140.37**	**569.03**	**371.99**	**221.60**
119	10	9	2.066E+07	1.736E+06	11.9000	147.5	**405.88**	**134.31**	**421.61**	**417.47**	**205.28**
271	16	24	1.764E+07	1.042E+06	16.9375	88.5	**570.28**	**147.94**	**583.20**	**396.58**	**232.38**
337	21	15	3.510E+07	2.188E+06	16.0476	185.9	**541.54**	**123.12**	**550.93**	**313.19**	**197.21**
358	19	40	1.398E+07	7.422E+05	18.8421	63.1	**631.36**	**150.11**	**643.19**	**385.06**	**237.68**
163	15	12	2.122E+07	1.953E+06	10.8667	166.0	**371.63**	**101.03**	**381.30**	**282.55**	**159.93**
172	17	12	2.240E+07	2.214E+06	10.1176	188.1	**346.69**	**88.89**	**354.74**	**242.35**	**142.22**
**********	**********	**********	**********	**********	**********	**********	**********	**********	**********	**********	**********
4618	304	342	2.110E+07	1.389E+06	15.1908	118.0	**513.75**	**34.88**	**514.36**	**61.68**	**55.04**
Pooled Ratio		15.1908	±	1.0314							
Mean Ratio		15.8209	±	1.0537							
Pooled Age		513.75	±	34.88	1 S.E.						
Mean Crystal Age		534.20	±	36.99	1 S.E.						
Binomial Age		514.36	+	61.68	"+95%"						
			-	55.04	"-95%"						
Central Age		**511.51**	**±**	**36.40**							
Age Dispersion		**9.31**	%								
Chi-squared		**24.748**	with	19	degrees of freedom						
P (Chi-Sq)		**16.90**	**%**								

Sample Number		**WYZ10**			Mineral	**Zircon**					
Position (#)		35			Glass (U pp	49.4					
Area of Graticule Squar		6.400E-07			Irradiation	UA-Z2					
No. of Crystals		20			Analyst	SNT					
Zeta Factor ± Error		121.1	3.5								
Rho d (% Relative Error)		5.799E+05	1.64								
N d		3711									
N s	N i	N g	Rho s	Rho i	Rho s / Rho	U ppm	Age (Ma)	Age error	50% Age	"+95%"	"-95%"
314	21	12	4.089E+07	2.734E+06	14.9524	232.9	**504.74**	**115.00**	**513.58**	**293.86**	**184.60**
512	32	21	3.810E+07	2.381E+06	16.0000	202.8	**538.66**	**99.77**	**544.77**	**236.14**	**163.34**
167	8	6	4.349E+07	2.083E+06	20.8750	177.5	**694.22**	**252.31**	**725.27**	**803.94**	**371.64**
311	25	24	2.025E+07	1.628E+06	12.4400	138.7	**422.64**	**88.98**	**429.04**	**222.40**	**145.02**
191	10	9	3.316E+07	1.736E+06	19.1000	147.9	**638.02**	**208.06**	**660.98**	**623.27**	**313.68**
308	24	12	4.010E+07	3.125E+06	12.8333	266.2	**435.56**	**93.44**	**442.40**	**234.89**	**151.82**
344	22	20	2.688E+07	1.719E+06	15.6364	146.4	**526.91**	**117.19**	**535.66**	**296.01**	**188.39**
534	31	25	3.338E+07	1.938E+06	17.2258	165.1	**578.13**	**108.52**	**584.82**	**256.97**	**176.98**
196	18	10	3.063E+07	2.813E+06	10.8889	239.6	**371.43**	**92.31**	**379.46**	**247.67**	**148.01**
257	17	12	3.346E+07	2.214E+06	15.1176	188.6	**510.10**	**128.86**	**521.16**	**343.60**	**204.00**
300	15	15	3.125E+07	1.563E+06	20.0000	133.1	**666.58**	**177.75**	**682.33**	**477.33**	**276.40**
212	12	8	4.141E+07	2.344E+06	17.6667	199.7	**592.27**	**176.84**	**610.16**	**506.86**	**271.45**
161	11	8	3.145E+07	2.148E+06	14.6364	183.0	**494.47**	**154.97**	**511.26**	**461.62**	**237.49**
421	30	20	3.289E+07	2.344E+06	14.0333	199.7	**474.83**	**91.10**	**480.69**	**219.43**	**149.33**
284	17	15	2.958E+07	1.771E+06	16.7059	150.9	**561.42**	**141.42**	**573.41**	**374.54**	**223.19**
352	35	20	2.750E+07	2.734E+06	10.0571	232.9	**343.80**	**62.00**	**347.66**	**148.01**	**103.22**
250	16	12	3.255E+07	2.083E+06	15.6250	177.5	**526.54**	**136.90**	**538.62**	**369.15**	**215.61**
324	19	15	3.375E+07	1.979E+06	17.0526	168.6	**572.57**	**136.49**	**583.46**	**352.70**	**216.85**
260	16	12	3.385E+07	2.083E+06	16.2500	177.5	**546.73**	**141.99**	**559.20**	**381.84**	**223.35**
465	45	25	2.906E+07	2.813E+06	10.3333	239.6	**352.99**	**56.34**	**356.05**	**129.56**	**94.58**
**********	**********	**********	**********	**********	**********	**********	**********	**********	**********	**********	**********
6163	424	301	3.199E+07	2.201E+06	14.5354	187.5	**491.18**	**29.58**	**491.61**	**49.52**	**44.97**
Pooled Ratio		14.5354	±	0.8752							
Mean Ratio		15.3715	±	0.6719							
Pooled Age		491.18	±	29.58	1 S.E.						
Mean Crystal Age		518.33	±	23.55	1 S.E.						
Binomial Age		491.61	+	49.52	"+95%"						
			-	44.97	"-95%"						
Central Age		**491.35**	**±**	**29.87**							
Age Dispersion		**3.52**	%								
Chi-squared		**17.456**	with	19	degrees of freedom						
P (Chi-Sq)		**55.90**	**%**								

Sample Number		**WYZ12**			Mineral	**Zircon**					
Position (#)		38			Glass (U pp	49.4					
Area of Graticule Squar		6.400E-07			Irradiation	UA-Z2					
No. of Crystals		18			Analyst	SNT					
Zeta Factor ± Error		121.1	3.5								
Rho d (% Relative Error)		5.769E+05	1.65								
N d		3692									
N s	N i	N g	Rho s	Rho i	Rho s / Rho	U ppm	Age (Ma)	Age error	50% Age	"+95%"	"-95%"
122	16	12	1.589E+07	2.083E+06	7.6250	178.4	**261.00**	**69.94**	**267.84**	**195.79**	**112.15**
77	15	8	1.504E+07	2.930E+06	5.1333	250.9	**176.87**	**50.26**	**182.36**	**144.98**	**80.90**
208	34	16	2.031E+07	3.320E+06	6.1176	284.3	**210.23**	**39.51**	**212.94**	**96.36**	**66.44**
118	24	10	1.844E+07	3.750E+06	4.9167	321.1	**169.50**	**38.37**	**172.81**	**99.99**	**63.70**
98	17	10	1.531E+07	2.656E+06	5.7647	227.5	**198.29**	**52.51**	**203.53**	**146.41**	**85.06**
291	57	40	1.137E+07	2.227E+06	5.1053	190.7	**175.91**	**26.14**	**177.33**	**59.52**	**44.84**
134	25	9	2.326E+07	4.340E+06	5.3600	371.7	**184.56**	**40.67**	**187.93**	**104.93**	**67.56**
175	24	16	1.709E+07	2.344E+06	7.2917	200.7	**249.80**	**55.01**	**254.19**	**141.64**	**90.60**
85	14	6	2.214E+07	3.646E+06	6.0714	312.2	**208.67**	**60.59**	**215.30**	**176.85**	**96.68**
217	34	28	1.211E+07	1.897E+06	6.3824	162.5	**219.18**	**41.08**	**221.97**	**100.05**	**69.01**
307	18	15	3.198E+07	1.875E+06	17.0556	160.6	**569.83**	**139.48**	**581.28**	**364.58**	**220.87**
148	24	12	1.927E+07	3.125E+06	6.1667	267.6	**211.89**	**47.16**	**215.77**	**122.08**	**77.93**
235	40	18	2.040E+07	3.472E+06	5.8750	297.3	**202.02**	**35.20**	**204.26**	**83.84**	**59.61**
147	34	20	1.148E+07	2.656E+06	4.3235	227.5	**149.28**	**28.84**	**151.42**	**70.97**	**48.82**
359	56	40	1.402E+07	2.188E+06	6.4107	187.3	**220.13**	**32.46**	**221.83**	**73.64**	**55.40**
132	27	16	1.289E+07	2.637E+06	4.8889	225.8	**168.55**	**36.04**	**171.48**	**91.91**	**60.21**
93	9	15	9.688E+06	9.375E+05	10.3333	80.3	**351.21**	**123.16**	**366.79**	**399.84**	**187.14**
113	24	12	1.471E+07	3.125E+06	4.7083	267.6	**162.41**	**36.90**	**165.62**	**96.27**	**61.31**
**********	**********	**********	**********	**********	**********	**********	**********	**********	**********	**********	**********
3059	492	303	1.577E+07	2.537E+06	6.2175	217.3	**213.61**	**12.57**	**213.79**	**21.23**	**19.36**
Pooled Ratio		6.2175	±	0.3660							
Mean Ratio		6.6406	±	0.6936							
Pooled Age		213.61	±	12.57	1 S.E.						
Mean Crystal Age		227.89	±	24.18	1 S.E.						
Binomial Age		213.79	+	21.23	"+95%"						
			-	19.36	"-95%"						
Central Age		**210.59**	**±**	**15.76**							
Age Dispersion		**18.78**	%								
Chi-squared		**32.815**	with	17	degrees of freedom						
P (Chi-Sq)		**1.19**	**%**								

Sample Number		**WYZ13**			Mineral	**Zircon**					
Position (#)		39			Glass (U pp	49.4					
Area of Graticule Squar		6.400E-07			Irradiation	UA-Z2					
No. of Crystals		20			Analyst	SNT					
Zeta Factor ± Error		121.1	3.5								
Rho d (% Relative Error)		5.754E+05	1.65								
N d		3682									
N s	N i	N g	Rho s	Rho i	Rho s / Rho	U ppm	Age (Ma)	Age error	50% Age	"+95%"	"-95%"
108	30	20	8.438E+06	2.344E+06	3.6000	201.2	**124.22**	**25.97**	**126.37**	**65.52**	**43.86**
258	35	28	1.440E+07	1.953E+06	7.3714	167.7	**251.84**	**46.13**	**254.85**	**111.38**	**77.36**
74	5	6	1.927E+07	1.302E+06	14.8000	111.8	**496.05**	**229.81**	**534.17**	**922.78**	**326.27**
218	27	24	1.419E+07	1.758E+06	8.0741	150.9	**275.34**	**56.92**	**279.53**	**142.97**	**94.13**
188	12	21	1.399E+07	8.929E+05	15.6667	76.7	**523.95**	**156.98**	**540.07**	**454.42**	**241.88**
120	18	12	1.563E+07	2.344E+06	6.6667	201.2	**228.18**	**58.17**	**233.66**	**159.33**	**94.32**
120	21	15	1.250E+07	2.188E+06	5.7143	187.8	**196.08**	**46.84**	**200.27**	**124.77**	**76.93**
248	23	16	2.422E+07	2.246E+06	10.7826	192.8	**365.13**	**80.51**	**371.30**	**205.79**	**131.12**
109	10	9	1.892E+07	1.736E+06	10.9000	149.1	**369.00**	**122.54**	**383.53**	**383.22**	**187.73**
312	39	30	1.625E+07	2.031E+06	8.0000	174.4	**272.87**	**47.22**	**275.74**	**111.87**	**79.38**
203	27	12	2.643E+07	3.516E+06	7.5185	301.8	**256.77**	**53.29**	**260.74**	**134.18**	**88.26**
182	30	20	1.422E+07	2.344E+06	6.0667	201.2	**207.97**	**41.56**	**211.03**	**103.47**	**69.50**
136	15	12	1.771E+07	1.953E+06	9.0667	167.7	**308.39**	**84.53**	**316.71**	**238.60**	**134.40**
220	26	20	1.719E+07	2.031E+06	8.4615	174.4	**288.26**	**60.54**	**292.78**	**152.84**	**99.83**
190	19	10	2.969E+07	2.969E+06	10.0000	254.9	**339.32**	**82.42**	**346.38**	**219.57**	**132.91**
181	11	18	1.571E+07	9.549E+05	16.4545	82.0	**549.21**	**171.53**	**567.54**	**506.67**	**262.01**
164	29	20	1.281E+07	2.266E+06	5.6552	194.5	**194.08**	**39.63**	**197.08**	**99.42**	**66.25**
81	9	9	1.406E+07	1.563E+06	9.0000	134.1	**306.18**	**108.06**	**320.13**	**353.71**	**164.75**
203	24	24	1.322E+07	1.563E+06	8.4583	134.1	**288.15**	**62.93**	**293.05**	**161.20**	**103.32**
184	25	20	1.438E+07	1.953E+06	7.3600	167.7	**251.46**	**54.25**	**255.69**	**138.60**	**89.53**
**********	**********	**********	**********	**********	**********	**********	**********	**********	**********	**********	**********
3499	435	346	1.580E+07	1.964E+06	8.0437	168.7	**274.32**	**16.67**	**274.58**	**28.50**	**25.85**
Pooled Ratio		8.0437	±	0.4887							
Mean Ratio		8.9809	±	0.7550							
Pooled Age		274.32	±	16.67	1 S.E.						
Mean Crystal Age		305.54	±	26.25	1 S.E.						
Binomial Age		274.58	+	28.50	"+95%"						
			-	25.85	"-95%"						
Central Age		**273.23**	**±**	**22.14**							
Age Dispersion		**23.38**	%								
Chi-squared		**40.790**	with	19	degrees of freedom						
P (Chi-Sq)		**0.26**	**%**								

Sample Number		**WYZ14**			Mineral	**Zircon**					
Position (#)		40			Glass (U pp	49.4					
Area of Graticule Squar		6.400E-07			Irradiation	UA-Z2					
No. of Crystals		20			Analyst	SNT					
Zeta Factor ± Error		121.1	3.5								
Rho d (% Relative Error)		5.739E+05	1.65								
N d		3673									
N s	N i	N g	Rho s	Rho i	Rho s / Rho	U ppm	Age (Ma)	Age error	50% Age	"+95%"	"-95%"
150	31	12	1.953E+07	4.036E+06	4.8387	347.4	**165.99**	**33.21**	**168.50**	**82.74**	**55.87**
127	13	8	2.480E+07	2.539E+06	9.7692	218.6	**330.84**	**96.97**	**341.01**	**282.89**	**152.25**
259	41	20	2.023E+07	3.203E+06	6.3171	275.7	**215.86**	**36.99**	**218.15**	**87.61**	**62.60**
282	18	20	2.203E+07	1.406E+06	15.6667	121.0	**522.64**	**128.24**	**533.28**	**337.23**	**203.63**
144	23	10	2.250E+07	3.594E+06	6.2609	309.3	**213.97**	**48.57**	**218.05**	**126.73**	**80.06**
114	22	16	1.113E+07	2.148E+06	5.1818	184.9	**177.60**	**41.78**	**181.32**	**110.57**	**68.94**
84	16	12	1.094E+07	2.083E+06	5.2500	179.3	**179.90**	**49.44**	**185.10**	**140.26**	**79.90**
189	16	14	2.109E+07	1.786E+06	11.8125	153.7	**397.94**	**104.45**	**407.50**	**286.63**	**165.81**
189	29	16	1.846E+07	2.832E+06	6.5172	243.8	**222.58**	**45.00**	**225.90**	**112.45**	**75.03**
102	15	9	1.771E+07	2.604E+06	6.8000	224.2	**232.07**	**64.64**	**238.75**	**184.65**	**103.43**
194	30	16	1.895E+07	2.930E+06	6.4667	252.2	**220.89**	**43.95**	**224.07**	**109.23**	**73.41**
500	16	30	2.604E+07	8.333E+05	31.2500	71.7	**1003.59**	**257.06**	**1024.52**	**651.99**	**394.26**
194	10	16	1.895E+07	9.766E+05	19.4000	84.1	**641.17**	**209.01**	**664.21**	**625.81**	**315.04**
125	28	15	1.302E+07	2.917E+06	4.4643	251.1	**153.30**	**32.45**	**155.93**	**82.44**	**54.42**
295	27	20	2.305E+07	2.109E+06	10.9259	181.6	**368.91**	**75.18**	**374.20**	**186.63**	**123.47**
251	26	24	1.634E+07	1.693E+06	9.6538	145.7	**327.03**	**68.25**	**332.02**	**171.43**	**112.20**
111	20	9	1.927E+07	3.472E+06	5.5500	298.9	**190.03**	**46.59**	**194.34**	**125.50**	**76.34**
333	34	30	1.734E+07	1.771E+06	9.7941	152.4	**331.66**	**60.72**	**335.51**	**145.82**	**101.07**
74	9	9	1.285E+07	1.563E+06	8.2222	134.5	**279.57**	**99.13**	**292.56**	**326.12**	**151.47**
96	12	12	1.250E+07	1.563E+06	8.0000	134.5	**272.17**	**83.83**	**281.64**	**252.37**	**131.37**
**********	**********	**********	**********	**********	**********	**********	**********	**********	**********	**********	**********
3813	436	318	1.874E+07	2.142E+06	8.7454	184.4	**296.95**	**17.97**	**297.23**	**30.62**	**27.78**
Pooled Ratio		8.7454	±	0.5293							
Mean Ratio		9.6071	±	1.4195							
Pooled Age		296.95	±	17.97	1 S.E.						
Mean Crystal Age		325.48	±	49.14	1 S.E.						
Binomial Age		297.23	+	30.62	"+95%"						
			-	27.78	"-95%"						
Central Age		**269.26**	**±**	**27.43**							
Age Dispersion		**36.18**	%								
Chi-squared		**88.206**	with	19	degrees of freedom						
P (Chi-Sq)		**0.00**	**%**								

Sample Number		**WYZ15**			Mineral	**Zircon**					
Position (#)		41			Glass (U pp	49.4					
Area of Graticule Squar		6.400E-07			Irradiation	UA-Z2					
No. of Crystals		16			Analyst	SNT					
Zeta Factor ± Error		121.1	3.5								
Rho d (% Relative Error)		5.724E+05	1.65								
N d		3663									
N s	N i	N g	Rho s	Rho i	Rho s / Rho	U ppm	Age (Ma)	Age error	50% Age	"+95%"	"-95%"
111	22	15	1.156E+07	2.292E+06	5.0455	197.8	**172.54**	**40.67**	**176.19**	**107.74**	**67.16**
204	10	18	1.771E+07	8.681E+05	20.4000	74.9	**670.89**	**218.44**	**694.82**	**651.07**	**328.72**
246	12	12	3.203E+07	1.563E+06	20.5000	134.8	**674.01**	**200.52**	**693.95**	**567.99**	**306.37**
188	40	16	1.836E+07	3.906E+06	4.7000	337.1	**160.87**	**28.52**	**162.77**	**68.32**	**48.50**
97	45	25	6.063E+06	2.813E+06	2.1556	242.7	**74.28**	**13.62**	**75.34**	**32.64**	**23.60**
64	14	8	1.250E+07	2.734E+06	4.5714	236.0	**156.52**	**46.48**	**161.93**	**137.00**	**74.61**
133	12	8	2.598E+07	2.344E+06	11.0833	202.3	**373.13**	**113.15**	**385.29**	**335.12**	**175.99**
153	9	9	2.656E+07	1.563E+06	17.0000	134.8	**563.81**	**194.29**	**586.82**	**608.35**	**291.34**
288	10	30	1.500E+07	5.208E+05	28.8000	44.9	**928.05**	**300.12**	**959.65**	**861.06**	**445.73**
364	16	60	9.479E+06	4.167E+05	22.7500	36.0	**743.87**	**191.62**	**760.05**	**502.16**	**298.03**
50	25	15	5.208E+06	2.604E+06	2.0000	224.7	**68.95**	**17.04**	**70.80**	**45.09**	**28.86**
134	7	21	9.970E+06	5.208E+05	19.1429	44.9	**631.50**	**245.74**	**664.35**	**830.16**	**358.45**
209	11	12	2.721E+07	1.432E+06	19.0000	123.6	**627.01**	**195.08**	**647.51**	**569.57**	**296.69**
199	16	25	1.244E+07	1.000E+06	12.4375	86.3	**417.27**	**109.32**	**427.21**	**299.16**	**173.31**
73	35	12	9.505E+06	4.557E+06	2.0857	393.3	**71.89**	**14.97**	**73.23**	**37.29**	**25.72**
130	20	15	1.354E+07	2.083E+06	6.5000	179.8	**221.44**	**53.70**	**226.25**	**143.92**	**87.70**
**********	**********	**********	**********	**********	**********	**********	**********	**********	**********	**********	**********
2643	304	301	1.372E+07	1.578E+06	8.6941	136.2	**294.50**	**20.35**	**294.88**	**36.86**	**32.79**
Pooled Ratio		8.6941	±	0.6008							
Mean Ratio		12.3857	±	2.1857							
Pooled Age		294.50	±	20.35	1 S.E.						
Mean Crystal Age		415.59	±	75.31	1 S.E.						
Binomial Age		294.88	+	36.86	"+95%"						
			-	32.79	"-95%"						
Central Age		**228.39**	**±**	**52.51**							
Age Dispersion		**88.07**	%								
Chi-squared		**259.735**	with	15	degrees of freedom						
P (Chi-Sq)		**0.00**	**%**								

Sample Number		**WYZ16B**			Mineral	**Zircon**					
Position (#)		42			Glass (U pp	49.4					
Area of Graticule Squar		6.400E-07			Irradiation	UA-Z2					
No. of Crystals		20			Analyst	SNT					
Zeta Factor ± Error		121.1	3.5								
Rho d (% Relative Error)		5.709E+05	1.65								
N d		3654									
N s	N i	N g	Rho s	Rho i	Rho s / Rho	U ppm	Age (Ma)	Age error	50% Age	"+95%"	"-95%"
127	21	8	2.480E+07	4.102E+06	6.0476	354.9	**205.74**	**48.95**	**210.07**	**130.19**	**80.31**
127	25	20	9.922E+06	1.953E+06	5.0800	169.0	**173.26**	**38.35**	**176.47**	**99.09**	**63.76**
266	21	16	2.598E+07	2.051E+06	12.6667	177.5	**423.63**	**97.05**	**431.26**	**250.55**	**156.59**
107	18	8	2.090E+07	3.516E+06	5.9444	304.2	**202.28**	**51.97**	**207.29**	**142.92**	**84.47**
75	9	6	1.953E+07	2.344E+06	8.3333	202.8	**281.82**	**99.86**	**294.87**	**328.35**	**152.54**
229	29	21	1.704E+07	2.158E+06	7.8966	186.7	**267.35**	**53.44**	**271.16**	**132.73**	**88.75**
106	17	12	1.380E+07	2.214E+06	6.2353	191.5	**212.02**	**55.84**	**217.51**	**155.32**	**90.32**
180	28	14	2.009E+07	3.125E+06	6.4286	270.4	**218.48**	**44.98**	**221.87**	**113.12**	**74.88**
138	14	10	2.156E+07	2.188E+06	9.8571	189.3	**332.04**	**93.79**	**341.49**	**268.35**	**148.09**
147	21	20	1.148E+07	1.641E+06	7.0000	142.0	**237.55**	**55.98**	**242.37**	**148.18**	**91.57**
121	22	8	2.363E+07	4.297E+06	5.5000	371.8	**187.37**	**43.87**	**191.24**	**115.94**	**72.32**
66	8	8	1.289E+07	1.563E+06	8.2500	135.2	**279.06**	**104.88**	**293.69**	**359.96**	**158.52**
194	25	12	2.526E+07	3.255E+06	7.7600	281.7	**262.82**	**56.53**	**267.18**	**144.20**	**93.20**
197	37	14	2.199E+07	4.129E+06	5.3243	357.3	**181.47**	**33.07**	**183.71**	**79.91**	**55.95**
85	15	12	1.107E+07	1.953E+06	5.6667	169.0	**192.97**	**54.42**	**198.79**	**156.51**	**87.42**
115	18	12	1.497E+07	2.344E+06	6.3889	202.8	**217.15**	**55.52**	**222.43**	**152.31**	**90.10**
344	46	20	2.688E+07	3.594E+06	7.4783	311.0	**253.46**	**40.68**	**255.76**	**94.33**	**68.85**
295	13	40	1.152E+07	5.078E+05	22.6923	43.9	**740.25**	**211.23**	**760.16**	**580.94**	**323.62**
145	20	21	1.079E+07	1.488E+06	7.2500	128.8	**245.87**	**59.22**	**251.07**	**158.13**	**96.50**
84	16	16	8.203E+06	1.563E+06	5.2500	135.2	**178.97**	**49.18**	**184.14**	**139.56**	**79.49**
**********	**********	**********	**********	**********	**********	**********	**********	**********	**********	**********	**********
3148	423	298	1.651E+07	2.218E+06	7.4421	191.9	**252.26**	**15.53**	**252.50**	**26.77**	**24.24**
Pooled Ratio		7.4421	±	0.4582							
Mean Ratio		7.8525	±	0.8794							
Pooled Age		252.26	±	15.53	1 S.E.						
Mean Crystal Age		265.89	±	30.33	1 S.E.						
Binomial Age		252.50	+	26.77	"+95%"						
			-	24.24	"-95%"						
Central Age		**244.43**	**±**	**19.38**							
Age Dispersion		**21.62**	%								
Chi-squared		**38.016**	with	19	degrees of freedom						
P (Chi-Sq)		**0.59**	**%**								

Sample Number		**WYZ18**			Mineral	**Zircon**					
Position (#)		43			Glass (U pp	49.4					
Area of Graticule Squar		6.400E-07			Irradiation	UA-Z2					
No. of Crystals		20			Analyst	SNT					
Zeta Factor ± Error		121.1	3.5								
Rho d (% Relative Error)		5.694E+05	1.66								
N d		3644									
N s	N i	N g	Rho s	Rho i	Rho s / Rho	U ppm	Age (Ma)	Age error	50% Age	"+95%"	"-95%"
163	18	15	1.698E+07	1.875E+06	9.0556	162.7	**304.89**	**76.40**	**311.72**	**206.89**	**123.07**
151	13	8	2.949E+07	2.539E+06	11.6154	220.3	**388.52**	**113.04**	**400.09**	**326.87**	**176.77**
145	28	20	1.133E+07	2.188E+06	5.1786	189.8	**176.11**	**36.82**	**179.01**	**93.19**	**61.57**
78	8	8	1.523E+07	1.563E+06	9.7500	135.6	**327.68**	**122.14**	**344.28**	**415.15**	**183.86**
149	24	20	1.164E+07	1.875E+06	6.2083	162.7	**210.57**	**46.84**	**214.42**	**121.28**	**77.41**
212	25	18	1.840E+07	2.170E+06	8.4800	188.3	**285.93**	**61.21**	**290.59**	**155.65**	**100.73**
230	42	30	1.198E+07	2.188E+06	5.4762	189.8	**186.09**	**31.84**	**188.09**	**75.44**	**54.08**
227	37	25	1.419E+07	2.313E+06	6.1351	200.6	**208.13**	**37.54**	**210.59**	**90.38**	**63.34**
258	38	25	1.613E+07	2.375E+06	6.7895	206.1	**229.93**	**40.68**	**232.52**	**97.26**	**68.56**
88	15	18	7.639E+06	1.302E+06	5.8667	113.0	**199.16**	**56.03**	**205.11**	**160.94**	**89.94**
72	18	18	6.250E+06	1.563E+06	4.0000	135.6	**136.45**	**36.25**	**140.27**	**100.87**	**59.38**
109	25	12	1.419E+07	3.255E+06	4.3600	282.4	**148.59**	**33.32**	**151.48**	**86.46**	**55.57**
159	18	21	1.183E+07	1.339E+06	8.8333	116.2	**297.57**	**74.66**	**304.28**	**202.38**	**120.34**
239	31	16	2.334E+07	3.027E+06	7.7097	262.6	**260.47**	**50.48**	**263.96**	**124.09**	**84.13**
151	26	12	1.966E+07	3.385E+06	5.8077	293.7	**197.19**	**42.38**	**200.57**	**108.33**	**70.44**
173	18	18	1.502E+07	1.563E+06	9.6111	135.6	**323.13**	**80.75**	**330.29**	**218.08**	**129.89**
187	16	16	1.826E+07	1.563E+06	11.6875	135.6	**390.86**	**102.64**	**400.27**	**281.92**	**163.00**
229	40	25	1.431E+07	2.500E+06	5.7250	216.9	**194.42**	**33.94**	**196.59**	**80.91**	**57.51**
172	15	18	1.493E+07	1.302E+06	11.4667	113.0	**383.69**	**104.09**	**393.59**	**290.56**	**164.60**
207	43	30	1.078E+07	2.240E+06	4.8140	194.3	**163.87**	**28.00**	**165.66**	**66.34**	**47.72**
**********	**********	**********	**********	**********	**********	**********	**********	**********	**********	**********	**********
3399	498	373	1.424E+07	2.086E+06	6.8253	181.0	**231.12**	**13.50**	**231.32**	**22.65**	**20.67**
Pooled Ratio		6.8253	±	0.3987							
Mean Ratio		7.4285	±	0.5533							
Pooled Age		231.12	±	13.50	1 S.E.						
Mean Crystal Age		251.16	±	19.05	1 S.E.						
Binomial Age		231.32	+	22.65	"+95%"						
			-	20.67	"-95%"						
Central Age		**231.26**	**±**	**17.07**							
Age Dispersion		**19.65**	%								
Chi-squared		**37.097**	with	19	degrees of freedom						
P (Chi-Sq)		**0.77**	**%**								

Sample Number		**WYZ22**			Mineral	**Zircon**					
Position (#)		44			Glass (U pp	49.4					
Area of Graticule Squar		6.400E-07			Irradiation	UA-Z2					
No. of Crystals		20			Analyst	SNT					
Zeta Factor ± Error		121.1	3.5								
Rho d (% Relative Error)		5.679E+05	1.66								
N d		3634									
N s	N i	N g	Rho s	Rho i	Rho s / Rho	U ppm	Age (Ma)	Age error	50% Age	"+95%"	"-95%"
186	42	20	1.453E+07	3.281E+06	4.4286	285.4	**150.51**	**26.20**	**152.24**	**62.41**	**44.68**
242	24	15	2.521E+07	2.500E+06	10.0833	217.5	**337.73**	**73.15**	**343.26**	**186.14**	**119.63**
139	26	15	1.448E+07	2.708E+06	5.3462	235.6	**181.26**	**39.20**	**184.45**	**100.44**	**65.26**
177	27	12	2.305E+07	3.516E+06	6.5556	305.8	**221.57**	**46.37**	**225.12**	**117.32**	**77.03**
100	16	10	1.563E+07	2.500E+06	6.2500	217.5	**211.41**	**57.36**	**217.23**	**161.84**	**92.38**
156	22	15	1.625E+07	2.292E+06	7.0909	199.3	**239.33**	**55.09**	**243.95**	**144.43**	**90.34**
147	29	16	1.436E+07	2.832E+06	5.0690	246.4	**171.99**	**35.41**	**174.74**	**89.13**	**59.34**
172	26	12	2.240E+07	3.385E+06	6.6154	294.5	**223.56**	**47.63**	**227.27**	**121.28**	**78.95**
141	25	9	2.448E+07	4.340E+06	5.6400	377.5	**191.08**	**41.95**	**194.52**	**108.10**	**69.62**
350	25	16	3.418E+07	2.441E+06	14.0000	212.4	**464.28**	**97.35**	**471.18**	**242.08**	**158.21**
216	36	15	2.250E+07	3.750E+06	6.0000	326.2	**203.09**	**37.18**	**205.57**	**89.94**	**62.69**
207	37	18	1.797E+07	3.212E+06	5.5946	279.4	**189.56**	**34.42**	**191.87**	**83.07**	**58.18**
358	48	21	2.664E+07	3.571E+06	7.4583	310.7	**251.49**	**39.56**	**253.68**	**91.22**	**67.04**
178	29	18	1.545E+07	2.517E+06	6.1379	219.0	**207.68**	**42.16**	**210.82**	**105.56**	**70.38**
211	33	18	1.832E+07	2.865E+06	6.3939	249.2	**216.20**	**41.11**	**219.04**	**100.63**	**68.98**
222	25	21	1.652E+07	1.860E+06	8.8800	161.8	**298.34**	**63.72**	**303.15**	**161.76**	**104.75**
134	12	12	1.745E+07	1.563E+06	11.1667	135.9	**372.98**	**113.07**	**385.12**	**334.88**	**175.86**
152	28	10	2.375E+07	4.375E+06	5.4286	380.6	**184.02**	**38.34**	**187.00**	**96.90**	**64.04**
310	36	20	2.422E+07	2.813E+06	8.6111	244.7	**289.51**	**51.88**	**292.76**	**124.12**	**86.82**
205	38	16	2.002E+07	3.711E+06	5.3947	322.8	**182.89**	**32.87**	**185.07**	**79.09**	**55.66**
**********	**********	**********	**********	**********	**********	**********	**********	**********	**********	**********	**********
4003	584	309	2.024E+07	2.953E+06	6.8545	256.9	**231.49**	**12.83**	**231.66**	**20.85**	**19.16**
Pooled Ratio		6.8545	±	0.3800							
Mean Ratio		7.1072	±	0.5305							
Pooled Age		231.49	±	12.83	1 S.E.						
Mean Crystal Age		239.87	±	18.22	1 S.E.						
Binomial Age		231.66	+	20.85	"+95%"						
			-	19.16	"-95%"						
Central Age		**226.93**	**±**	**15.86**							
Age Dispersion		**18.78**	%								
Chi-squared		**38.565**	with	19	degrees of freedom						
P (Chi-Sq)		**0.50**	**%**								